ED1-1-INV

Towards the quantum limit with Josephson traveling wave parametricamplifiers

*Kevin P. O'Brien[1]

Massachusetts Institute of Technology[1]

We detail recent advances in Josephson junction based parametricamplifiers, including traveling wave and impedance engineered cavitybased amplifiers. We provide an overview and tutorial on usingJosephsonCircuits.jl, our Julia package for high performance simulationsof the gain and quantum efficiency of arbitrary circuits containingJosephson junctions, including the impact of an arbitrary number ofpump, signal, and idler modes, as well as dielectric loss. We describehow Floquet mode traveling wave parametric amplifiers suppress thegeneration of unwanted modes, yielding higher quantum efficiency andless sensitivity to the impedance environment outside of theamplification band. Finally, we describe our progress towards realizingnear ideal quantum efficiency Floquet mode Josephson traveling waveparametric amplifiers in a low loss aluminum process.

Keywords: Qubit

ED1-2-INV

A novel technique for the spectroscopy of parasitic defects in superconducting qubits

*Leonid Abdurakhimov[1], Imran Mahboob[1], Hiraku Toida[1], Kosuke Kakuyanagi[1], Yuichiro Matsuzaki[2], Shiro Saito[1]

NTT Basic Research Laboratories, NTT Corporation, Japan[1]
AIST, Japan[2]

Superconducting qubits are among the most promising platforms for building a quantum computer. Despite tremendous progress in recent years, the realization of a fault-tolerant quantum computer remains a challenging task due to limited lifetimes of superconducting qubits. One of the major noise mechanisms limiting qubit lifetimes is the interaction between a qubit and unwanted two-level-system (TLS) defects. TLS defects are various atomic-scale defects of different microscopic nature which are mainly formed in amorphous layers such as the aluminum-oxide tunnel barrier of an Al/AlOx/Al Josephson junction. Those defects can be phenomenologically modelled as quantum systems with two energy levels, and, conventionally, it is assumed that the dominant type of TLS defects are charge defects that are coupled to a superconducting qubit via fluctuations of the electric charge induced on superconducting islands.

In this work, we introduce a novel method of TLS defect spectroscopy in superconducting qubits that allows one to distinguish different types of TLS defects [1]. In particular, we report the observation of TLS defects coupled to a superconducting qubit through fluctuations of the critical current through a Josephson junction. This type of defect-qubit interaction was discussed theoretically in the literature, but up to the present it has not been reliably observed in experiments. The distinctive feature of critical-current-induced TLS defects is that the interaction between such defects and a superconducting qubit is described by a nonlinear term $\sim\cos(\varphi) \sim\varphi^2$ for a small superconducting phase difference across the Josephson junction φ.

Our technique of defect detection is based on the resonant AC Stark effect (Autler-Townes splitting) induced by the application of a strong microwave drive at a qubit resonance frequency [1,2]. According to our theoretical model, the resonance interaction between a strongly driven qubit and a TLS defect is realized in the rotating frame when a particular relation between the qubit drive amplitude Ω (the Rabi frequency), qubit frequency ω_q, and defect frequency ωtls is met. For TLS defects coupled to a qubit via charge fluctuations, the resonance condition is given by the equation $\Omega=|\omega_{tls} - \omega_q|$. For TLS defects coupled to a qubit via critical current fluctuations, the resonance condition is given by the expression $\Omega=|\omega_{tls} - 2\omega_q|$. By measuring defect spectral signatures at different values of the applied magnetic flux, we were able to distinguish critical-current-coupled defects from standard TLS defects with the charge-fluctuation coupling.

Our test qubit is a capacitively-shunted flux qubit coupled to a 3D microwave cavity [3]. The qubit consists of the aluminum superconducting loop interrupted by three Al/AlOx/Al Josephson junctions with one of the junctions being shunted by a large capacitance. The qubit frequency can be tuned by applying an external magnetic flux through the qubit loop. At the optimal point of the magnetic flux bias, the qubit is insensitive to the magnetic flux noise to the first order, and the qubit energy-relaxation and dephasing times are close to 100 μs [3]. We detected TLS defect signatures by measuring the qubit population after a long resonant drive pulse as a function of

the qubit frequency and drive amplitude. We found that signatures of charge-fluctuation TLS defects follow the qubit frequency value, while signatures of critical-current TLS defects follow the double value of the qubit frequency, in accordance with the theoretical model.

The reported technique of TLS defect spectroscopy can be extended to other types of superconducting qubits, and, hence, it will be a valuable tool for quantifying TLS defects and finding optimal techniques and materials for the fabrication of defect-free qubits.

This work was supported by JST CREST (JPMJCR1774) and JST Moonshot R&D (JPMJMS2067).

[1] L. V. Abdurakhimov, I. Mahboob, H. Toida, K. Kakuyanagi, Y. Matsuzaki, S. Saito, "Identification of different types of high-frequency defects in superconducting qubits", arXiv:2112.05391 (2022).
[2] L. V. Abdurakhimov, I. Mahboob, H. Toida, K. Kakuyanagi, Y. Matsuzaki, S. Saito, "Driven-state relaxation of a coupled qubit-defect system in spin-locking measurements", Phys. Rev. B 102, 100502 (2020).
[3] L. V. Abdurakhimov, I. Mahboob, H. Toida, K. Kakuyanagi, S. Saito, "A long-lived capacitively shunted flux qubit embedded in a 3D cavity", Appl. Phys. Lett. 115, 262601 (2019).

Keywords: superconducting qubit, defect, critical current, microwave spectroscopy

ED1-3

Study of Superconducting Qubit Frequency Estimation Method

*Shingo Tokunaga[1,3], Shinichi Hirose[1,3], Shuhei Tamate[2], Yutaka Tabuchi[2], Norinao Kouma[1,3], Yoshiyasu Doi[1,3], Shintaro Sato[1,3], Yasunobu Nakamura[2,3,4]

Fujitsu Limited, Japan[1]
RIKEN Center for Quantum Computing (RQC), Japan[2]
RIKEN RQC-FUJITSU Collaboration Center, Japan[3]
Department of Applied Physics, Graduate School of Engineering, The University of Tokyo, Japan[4]

Superconducting quantum computers are expected to have a lot of identical qubits. Avoiding frequency collision is one of the most important challenges in fixed-frequency-transmon-qubit architectures, given that the spurious hybridization causes an error in quantum gates with smaller detuning between nearest and next-nearest neighboring qubits.

To achieve high-fidelity gates, the qubit frequencies should be well assigned in design and fabrication, and unavoidable fabrication errors are removed by the post-tuning process [1]. In reference [1], they tune the critical current of a Josephson junction by irradiating laser pulses with feedback of the normal resistance under the assumption that the resistance and the qubit frequency have 1-to-1 correspondence. Thus, high-precision estimation of the qubit frequencies at room-temperature is getting in the heart of quality improvement of an entire system. However, there is another factor to deviate the qubit frequencies.

According to the formula (B1) in [2], the factors determining the qubit frequency are the capacitance of the electrodes and the junction inductance. We estimate the capacitance from the shape of the electrodes, and we can infer the inductance of the Josephson junction from two parameters: the superconducting gap Delta of the metal used for the junction and the normal-state resistance R_N of the junction measurable at room temperature [3]. Even If the normal-state resistance R_N of the junction is controlled with laser annealing, superconducting gap fluctuation unmeasurable at room temperature may limit the accuracy of the qubit frequencies.

Here, we focus on whether we can accurately find qubit frequency using the same fabrication conditions and the junction resistance R_N in room temperature measurements. To clarify the relationship between the R_N and the qubit frequency, we evaluated the fluctuation of the product of the critical current I_C
obtained in low-temperature measurement and junction resistance R_N measured at room temperature. We experimentally obtained that I_CR_N variation was almost less than 1%. For instance, we try to minimize the frequency variation below 0.5% (1.0% fluctuation for both R_N and I_CR_N) for all-working 64 qubits in our 8x8 lattice. We found that the variation was almost on the border of our criteria.

We found qubits having relatively large I_CR_N deviation as exceptions. They show larger thickness variation in the oxidization layer in the Josephson junction (through TEM measurements) and show broader line widths observed at the qubits of g-e transition (shorter coherence time). We will discuss that reason and strategy for the improvement.

[1] J. B. Hertzberg, E. J. Zhang, S. Rosenblatt, E. Magesan, J. A. Smolin, J.-B. Yau, V. P. Adiga, M. Sandberg, M. Brink, and J. M. Chow et al., Laser-Annealing Josephson Junctions for Yielding Scaled-up Superconducting Quantum Processors, arXiv:2009.00781.
[2] Nicolas Didier, Analytical modeling of parametrically-modulated transmon qubits, Phys. Rev. A 97, 022330 (2018)
[3] Vinay Ambegaokar, Alexis Baratoff, Tunneling Between Superconductors, Phys. Rev. Lett. 10, 486 (1963)

Keywords: quantum, Josephson, superconducting gap

ED1-4

Design of an on-chip cross-resonance filter

*Mitsuya Kawashita[1,3], Shuhei Tamate[2], Yutaka Tabuchi[2], Norinao Kouma[1,3], Yoshiyasu Doi[1,3], Shintaro Sato[1,3], Yasunobu Nakamura[2,3,4]

Fujitsu Limited, Japan[1]
RIKEN Center For Quantum Computing (RQC), Japan[2]
RIKEN RQC-FUJITSU Collaboration Center, Japan[3]
Department of Applied Physics, Graduate School of Engineering, The University of Tokyo, Japan[4]

The number of quantum bits embedded in superconducting quantum computers is rapidly increasing. However, there are still many challenges for achieving a continuous increase in the number of qubits. One of the crucial requirements is to reduce the size of electrical instruments for controlling qubits [1]. In general, quantum computers require separate electronic circuits for a single-qubit gate and a two-qubit gate. This has increased the scale of electronic circuits. If two kinds of control signals for a single-qubit gate and two-qubit gate can be output from one electronic apparatus, the scale of the electronic apparatus is reduced. The control signals for the two-qubit gate are frequency-multiplexed microwave signals. By applying the wideband DA converter to electrical instruments, the band of the control signal can be output from one electrical instrument. However, since the amplitude difference between the single-qubit gate and the two-qubit gate is large, it is difficult to adjust the amplitude difference only by electrical instruments.

In this study, we design an on-chip filter that can suppress the amplitude of the microwave for a single-qubit gate and transmit that for a two-qubit gate in order to compensate for the difference in amplitudes required for the single-qubit gate and two-qubit gate. The difference in amplitude guaranteed by the filter must be at least 20 dB. To create a high-pass filter with 20 dB attenuation, we used a technique to make both bandpass and notch with a single resonator [3]. In oursample, an input microwave signal for controlling the qubit is transferred from the back of the chip. To realize a compact on-chip filter, the filter was designed on the backside of the chip with a single resonator. Simulations using the circuit model show a difference in amplitude of more than 20 dB between the single-qubit and two-qubit gate, and a bandwidth of 100 MHz on the single-qubit gate side and 500 MHz on the two-qubit side with relatively flat characteristics. We will report on the performance of the on-chip filter using the electromagnetic field simulator COMSOL.

[1] Almudever, Carmen G., et al. "The engineering challenges in quantum computing." Design, Automation & Test in Europe Conference & Exhibition (DATE), 2017. IEEE, 2017.
[2] J.M. Chow, et al. "A simple all-microwave entangling gate for fixed-frequency superconducting qubits“ Physical Review. Lett. 107, 080502 (2011).
[3] Bronn, Nicholas T., et al. "Reducing spontaneous emission in circuit quantum electrodynamics by a combined readout/filter technique." IEEE Transactions on Applied Superconductivity 25.5 (2015): 1-10.

Keywords: Quantum Computer, Cross Resonance, Filter

ED2-1-INV

Ultrasonic Guided Wave Testing for Pipes using HTS-SQUID

*Yoshimi Hatsukade[1], Kohei Okada[1], Temuulen Munkhnyam[1], Ryohei Ohwa[1], Wenxu Sun[1]

Kindai University[1]

There are countless pipelines in facilities of such as oil and gas, chemical processing, and related industries. Steel tube pipe general (STPG) for pressure service is a commonly used pipe, and they are jacketed with thermal insulations. Due to penetration of water, corrosion under insulation (CUI) that occurs on surface of the pipe is a major problem. At present, it is difficult to detect the CUIs without removal of the insulations from the pipes by conventional non-destructive testing (NDT) technique.

Therefore, we have developed a novel non-contacting ultrasonic guided wave testing (UGWT) technique that enables us to inspect defects on the STPG pipes in the insulation. To realize this inspection, we developed a magnetostriction-based UGWT technique, which utilized the magnetostrictive effects of the STPG pipe itself. In this method, we use electromagnets to give remnant magnetic field in the pipe, at which the magnetostrictive effect occurs by applying pulse magnetic field, leading to generation of guided wave. We utilized a high-sensitive HTS-SQUID gradiometer to receive magnetic signal generated at the remnant field by the inverse magnetostrictive effect due to the guided wave propagating in the pipe.

In this talk, we firstly introduce the conventional magnetostriction-based UGWT technique, which pastes nickel thin films on a pipe as magnetostrictive transducer. We developed this technique to the non-contacting UGWT technique using the remnant field of the pre-magnetized STPG370 pipe in place of the nickel film. Pre-magnetization conditions, such as shape of the electromagnets, current amplitude to the electromagnets, were derived from electromagnetic field simulation. We demonstrated non-contacting transceive of T(0, 1) mode guided waves using the novel technique. We also demonstrated defect detection using this technique and discuss feasibility of this technique for practical use.

Keywords: steel tube pipe general, magnetostrictive effects, ultrasonic guided wave testing, HTS-SQUID gradiometer

ED2-2-INV

Magnetic immunoassay with SQUID and magnetic marker

*Charles Shieh-Yueh Yang[1]

MagQu Co., Ltd[1]

In order to have high sensitivity and specificity, the assay technology so-called immunomagnetic reduction (IMR) was developed in 2006. The reagent of IMR assay is composed of antibody functionalized magnetic Fe3O4 nanoparticles (diameter ~ 55 nm) dispersed in phosphate buffered saline. Once the magnetic nanoparticles bind with target biomarkers, the alternative-current (AC) magnetic susceptibility of reagent is reduced. Samples with ultra-low concentrated biomarkers show very tiny reductions in the AC magnetic susceptibility of reagent. An ultra-sensitive sensor is needed. High-temperature (high-Tc) superconducting quantum interference device (SQUID) magnetometer is a candidate to precisely sense tiny changes in magnetic signals. IMR analyzer utilizing a high-Tc SQUID magnetometer was developed in 2008. The IMR assay system including reagent and analyzer has been applied to quantitatively detect blood biomarkers, which concentrations are fg/ml - pg/ml, associated with Alzheimer's disease (AD), Parkinson's disease (PD) and frontotemporal dementia (FTD) since 2012. Up to now, there have been more than 80 papers of clinical evidence in Asian, American and Europe to demonstrate the feasibilities of using IMR system in clinics. The accuracy of finding early-stage AD, PD or FTD is higher than 80%. IMR system for assaying blood biomarkers of dementia were approved as an in-vitro medical device in Taiwan and Europe in 2020. It opens a new era to screen neurodegenerative diseases via blood draw instead of lumbar puncture. In this work, we would like to give an overview from the developments of IMR assay system to the clinical applications in assessing neurodegenerative diseases via assaying blood biomarkers.Correspondence: Charles S.Y. Yang (email: syyang@magqu.com)

Keywords: immunomagnetic reduction, superconducting quantum interference device, biomarkers, neurodegenerative disease

ED2-3-INV

A SQUID biomagnetic measurement system for magnetospinography and magnetoneurography

*Yoshiaki Adachi[1], Shigenori Kawabata[2]

Kanazawa Institute of Technology[1]
Tokyo Medical and Dental University[2]

We developed a SQUID biomagnetic measurement system for magnetospinography/magnetoneurography (MSG/MNG). Biomagnetic measurement is a promising method to noninvasively obtain functional information of neurons or muscles in a living body. Weak magnetic fields elicited by their electric activities were captured by highly sensitive magnetic flux sensors arranged along the body surface. The current distribution was estimated by appropriate source reconstruction algorithm applied to the obtained magnetic field distribution. The estimated current distribution overlaied on the anatomical image acquired by magnetic resonance imaging (MRI) or radiographic imaging is informative in terms of neuromuscular function and contributes a lot to the accurate diagnoses of neurological disorders.

The intensity of biomagnetic fields observed on the body surface are quite small and ranging from several fT to several tens pT. Therefore, superconducting quantum interference device (SQUID)-based magnetic flux sensors are practically applied to the detection of the biomagnetic fields. Various SQUID-based measurement systems for magnetoencephalograph (MEG) and magnetocardiograph (MCG) are already commercialized and introduced to hospitals for diagnoses of the brain/heart diseases.

As well as the conventional SQUID-based biomagnetic measurement systems such as MEG or MCG, the measurement system for MSG/MNG is equipped with an array of SQUID sensors, a cryostat to keep superconducting state of the sensors, electronics to linearization and dynamic range enhancement of the sensor outputs, a digital data acquisition unit with filters, and PCs for control and analysis.

However, to detect MSG/MNG signals that are smaller and faster than MEG signals, various improvements were added to the measurement system; the sensor array composed of vector-type SQUID gradiometers, the uniquely-shaped cryostat, and a digital data acquisition unit with higher sampling rate. Especially, the cryostat design was optimized for fitting the sensor array to the posterior of a supine subject. The cryostat composed of a cylindrical main body to reserve liquid helium (LHe) and the horizontal protrusion from its side surface. The SQUID sensor array oriented vertically was installed in the protrusion along its upper surface. The magnetic signals from any part of the body can readily be obtained as long as the subject placed a certain body part on the protrusion. Additionally, owing to the structure of the cryostat, on-site X-ray imaging became applicable to obtain the skeletal structure of the subject from lateral and anterior sides. The obtained X-ray image was effective for positioning a subject and further magnetic source analysis.

Whenever we introduced a SQUID-based system to a hospital, the operational cost of the LHe consumption became a large inevitable problem so far. To solve the problem of the LHe cost, we combined the MSG/MNG system with a closed-cycle helium recondensing system, which could

recycle almost 100% of LHe. It enabled the system to work without refilling LHe for more than one year and drastically suppressed its operational cost.

The prototype of the MSG/MNG system is continuously being operated at the Tokyo Medical and Dental University hospital for years under the cooperation between medicine and engineering. In addition to the development of the hardware of the system, various software for analysis and visualization were also developed based on innovative ideas proposed from the medical staffs operating the MSG/MNG system. In particular, "the virtual electrodes" arranged along the neural pathways in the computer can display the behavior of the current distribution estimated from the magnetic field in waveforms. The waveforms from the virtual electrodes make the data obtained by the MSG/MNG easy to understand for physicians familiar with conventional electrophysiological testing and effective in diagnosing the site of the lesion.

Through our recent studies, we have successfully observed and evaluated nerve activities in the cervical, lumbar, thoracic, shoulder, elbow, and palmar areas, using the MSG/MNG system. In the future, the MSG/MNG is expected to spread as a new diagnostic tool for neurological diseases obtaining the functional information of nerves in every body part.

Keywords: SQUID, Biomagnetism, Magnetospinograph, Magnetoneurograph

ED2-4

Dispersion method of magnetic nanoparticles by femtosecond laser pulses for quantitative magnetic immune assay using HTS-SQUID

*Taiki Yamamoto[1], Kouhei Kishimoto[1], Hiroto Kuroda[1], Rekka Moriya[1], Kei Yamashita[1], Jin Wang[1], Kenji Sakai[1], Toshihiko Kiwa[1]

Okayama University (Japan)[1]

A magnetic immunoassay (MIA) has attracted attention of a lot of researchers since it is expected to realize a rapid and high-sensitive medical diagnosis. The MIA utilizes magnetic nanoparticles (MNPs), which generally show superparamagnetic properties, functionalized with antibodies to react with specific antigens. When the MNPs are conjugated with antigens in solutions, an AC magnetic susceptibility of MNPs decreases due to an increment in the particle volume. Thus, the concentration of the antigens could be measured by measuring the magnetic signals from the MNPs. Recently, a magnetic immunoassay system using high-T_c SQUIDs has been developed [1]. This system measures the third harmonic of the magnetic signals from the MNPs by applying the AC magnetic field with the frequency of 1.06 kHz and the amplitude of 8.5 mT_{p-p}. A first-order differential coil was mounted coaxially with an excitation coil to detect the signals. The detected signals were transferred to the planar superconductive coils magnetically coupled with an HTS-SQUID chip after being amplified by a lock-in circuit. We used ramp-edge junctions made from $SmBa_2Cu_3O_y$ (SmBCO) and $La_{0.1}$-$Er_{1.95}Cu_3O_y$ (La-ErBCO) for the HTS-SQUID. The sample solution in a quartz tube was located along the center axis of the coils.

However, the AC magnetic susceptivity of MNPs also decreases by aggregation of the MNPs, and it is difficult to distinguish the reduction of the signals by the conjugation from the signals by the aggregation. Therefore, quantitative measurement of the MIAs was challenging.

In our group, nonthermally dispersion of MNPs, driven by irradiating aggregated MNPs with femtosecond laser pulses [2], has been proposed. In this study, to introduce femtosecond laser pulses to the MIA system, a multimode optical fiber cable was installed along the central axis of the coils. Thus, measurement of the magnetic signals during the laser pulse irradiation could be realized.

The multimode fiber with a core diameter of 105 μm was used, which was connected to the femtosecond laser, which produced the laser pulses with a pulse width of 150 fs at FWHM, the center wavelength of 780 nm, and the repetition rate was 70 MHz, respectively.

Figure 1 shows the time evolution of the magnetic signal intensity of MNPs during the femtosecond laser irradiation. The diameter of MNPs was 180 nm in average. The concentration of sample particles was 2 mg/ml in 50 μl. The MNPs were firstly sonicated, and after leaving the sample for 35 min., we started laser irradiation (the start time was indicated as 3 min in Fig.1.). The signal intensities plotted in Fig.1 were normalized at the time is zero. The magnetic signal intensity increased by the laser irradiation due to the dispersion of the magnetic particles. The change in the signal intensity was proportionally increased by increasing the average power of the femtosecond laser pulses. The ratio of the signal at 45 min to 0 min were respectively 5.3%, 15.7%, and 31.8% for 5 mW, 10mW, and 25 mW. This result indicates that the dispersion of MNPs by the femtosecond laser during the measurements was realized.

[1]Mizoguchi *et al.,* IEEE Trans.Appl.Supercond,Vol.26,No.5,August 2016
[2] K. Kishimoto *et al.,* Presented at the 34th International Symposium on Superconductivity (ISS 2021), 30 Nov– 2 Dec, On-line, ED2-3

Fig.1 Laser output dependence of signal recovery

Keywords: Magnetic nano particles, SQUID, Magnetic immunoassay

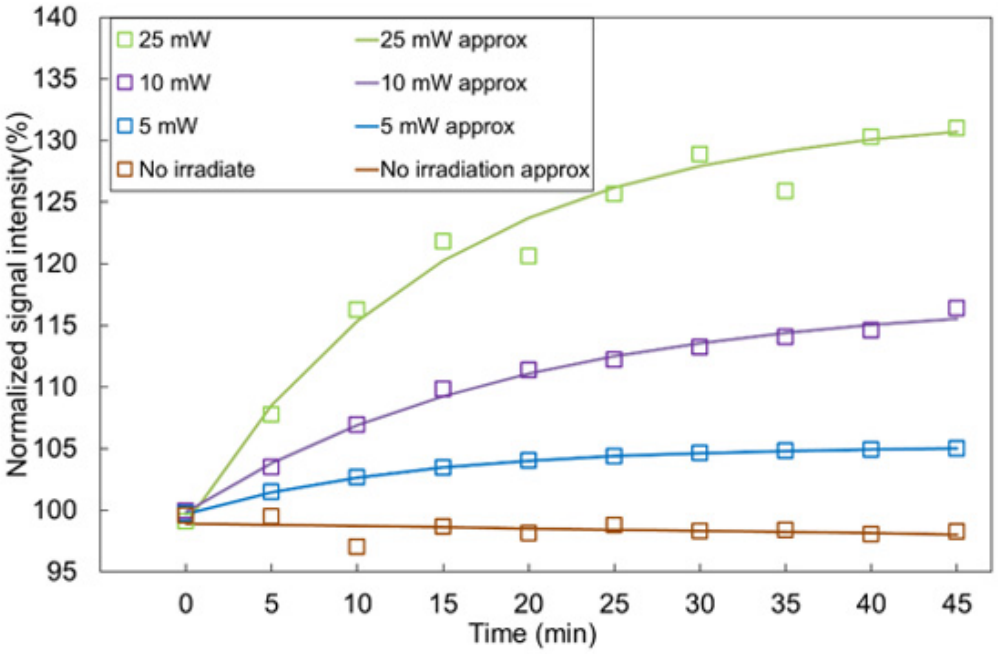

ED3-1-INV

Multi-pixel Gamma-Ray Transition-Edge Sensor Covering Wide Energy Range

*Takahiro Kikuchi[1], Go Fujii[1], Ryota Hayakawa[1,2], Ryan Smith[3], Fuminori Hirayama[1], Yasushi Sato[1], Satoshi Kohjiro[1], Masahiro Ukibe[1], Ohno Masashi[3], Akira Sato[1], Hirotake Yamamori[1], Takumi Hamaguchi[4], Takashi Yasumune[4], Chikara Ito[4], Koji Takasaki[4]

National Institute of Advanced Industrial Science and Technology (Japan)[1]
Tokyo Metropolitan University (Japan)[2]
University of Tokyo (Japan)[3]
Japan Atomic Energy Agency (Japan)[4]

Gamma-ray spectroscopy is suitable for non-destructive analysis of nuclear materials important for nuclear fuel cycles and global security. Transition-edge sensors (TESs) exhibit typically 10 times higher energy resolution (ΔE) than that of popular High Purity Germanium (HPGe) detectors. In low-energy range (20 keV< E < 220 keV), TESs with 236 pixels show 40 eV< ΔE < 60 eV suitable for measuring isotopic composition of nuclear materials [1,2]. On the other hand, there is a demand in high-energy range (E > 220 keV), such as detection of cesium (^{137}Cs) or positron-annihilation spectroscopy [3,4]. However, to our knowledge, there are no reports on multi-pixel TESs operating in this energy range.

We have been developing multi-pixel TESs applicable for both energy range. A unique improvement in our fabrication is a 7-μm thick $SiO_2/Si_xN_y/SiO_2$ membrane [5] with the same thermal conductance (≈1.5 nW/K) as conventional 1-μm thick silicon-nitride (Si_xN_y) membranes [1,6]. We expect that this thick membrane is more robust to support the heavier-metal absorber required for stopping higher energy photons and converts them into heat. In the low-energy range, a TES with a 0.5-mm-cubic Sn absorber shows 40 eV < ΔE < 47 eV at 86.5 keV for 4 pixels read out by our microwave SQUID multiplexer (MW-Mux) [7, 8]. It clearly separates two lines of neptunium (^{237}Np) at 86.5 keV and protoactinium (^{233}Pa) at 86.6 keV that HPGe cannot distinguish [9]. Moreover, their peak ratio agrees with the expectation based on the radio-active equilibrium between the two nuclides. In the high-energy range, another TES with a 0.8-mm-cubic Sn absorber shows 182 eV < ΔE < 290 eV at 320 keV for 6 pixels. Their ΔE are expected to be high enough for applications introduced above. These results are a milestone for gamma-ray spectrometers equipped with the large number of pixels. We will realize it, incorporating several TES and MW-Mux chips in the same measurement module [10].

[1] D. A. Bennet et al., Rev. Sci. Instrum, 83, 093113, 2012
[2] J. A. Ullom et al., Supercond. Sci. Technol. 28, 084003, 2015
[3] M. Ohno et al., IEICE Trans. Electron., 100, 283, 2017
[4] S. W. Leman et al., J. Low Temp. Phys., 151, 784, 2008
[5] T. Kikuchi et al., Appl. Phys. Lett., 119, 222602, 2021
[6] H. F. C. Hoevers et al., Appl. Phys. Lett., 86, 251903, 2005
[7] Y. Nakashima et al., IEEE Trans. Appl. Supercond. 29, 2100705, 2019
[8] Y. Nakashima et al., Appl. Phys. Lett., 117, 122601, 2020
[9] T. Kikuchi et al., J. Low Temp. Phys., Accepted.
[10] J. A. B. Mates et al., Appl. Phys. Lett., 111, 062601, 2017

Keywords: Transition Edge Sensor, Gamma ray, Trilayer Membrane, Spectroscopy

ED3-2

Fabrication of sub-5μm size small Ir-TES for infrared photon detection.

*Takeshi Jodoi[1], Yuki Mitsuya[1], Ryan Smith[1], Hiroyuki Takahashi[1]

School of Engineering, The University of Tokyo[1]

To realize optical quantum computer, it is required to develop a photon-number-resolving detector with small time jitter in the near infrared or communication wavelength. Transition Edge sensors (TESs) are promising photon-number-resolving detectors for near infrared photons, which can realize high energy resolution, a low time energy threshold, a high quantum efficiency, and a low dark count rate. TESs can show better energy resolution by lowering the transition temperature and reducing the heat capacity. In this study, we plan to improve the performance of the TES by reducing the heat capacity of the TES and evaluate the energy resolution and the photon number resolution,
We formed a silicon wafer into a racket-like shape which matches the inner diameter of optical fiber sleeve in order to improve the alignment between optical fiber and the sensitive area of TES.

Fig. 1 shows a setup of the detector with a magnified image of the fabricated TES.

We have fabricated 1μm x 1μm, 2μm x 2μm , 3μm x 3μm TESs. We will show the characteristics and energy resolution of these TESs

Keywords: Transition Edge Sensors, infrared single photon, photon number resolving, microfabrication

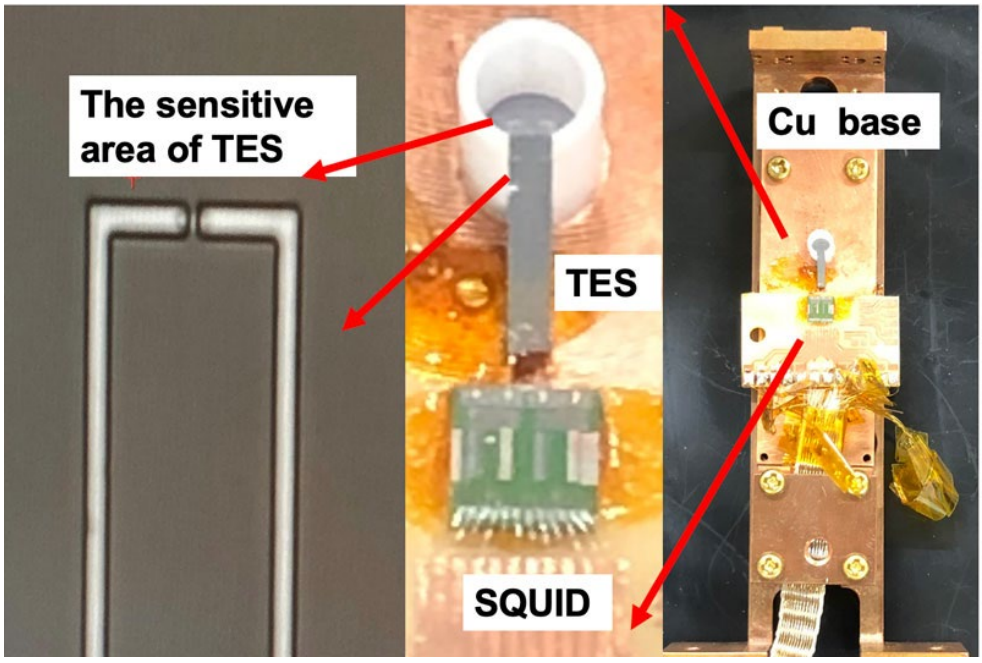

ED3-3

Study of the athermal phonon hot spot with superconducting Transition Edge Sensor

*Lorenzo Ferrari Barusso[1,2], Corrado Boragno[1], Edvige Celasco[1], Giovanni Gallucci[2], Daniele Grosso[1], Manuela Rigano[1], Flavio Gatti[1,2]

University of Genoa[1]
INFN Genoa[2]

Cryogenic focal plane anti-coincidence detector for X-ray space applications, as the Athena mission, with a large area (4 cm^2) silicon suspended absorber sensed by a network of 400 Ir/Au Transition Edge Sensors (TES) and connected through silicon bridges to a surrounding silicon frame plated with gold. The device is shaped by Deep Reactive Ion Etching from a single silicon wafer of 500 μm thickness. Fast response to the cosmic particle detection is achieved if the athermal phonon hot spot interact with TES in the signal generation. This have been highlighted in operating test of prototypes of the Demonstration Model of the CryoAC. To overcome the localized distribution of the athermal phonon hot spot the absorber area must be covered with a TES array having a defined pitch size. We are going to present the expectations of phonon simulation model and the measurement method of the phonon hot spot size that is predicted by the particle-absorber interaction model and define the TES array pitch size.

Keywords: superconducting Transition Edge Sensors, Phonon, particle detector

ED3-4

Study of fast single photon superconductive detector (SPSD) with Iridium/Gold bilayer at 0.1 K

*Edvige Celasco[1,2], Lorenzo Ferrari Barusso[1,2], Giovanni Gallucci[2], Daniele Grosso[1,2], Pietro Manfrinetti[1], Luca Repetto[1], Marine Schott[1], Kifayat Niazi[1], Favio Gatti[1,2]

Physics Dept University of Genoa[1]
Infn Genoa[2]

Driven by studies on quantum cryptography and nuclear decays, we developed an iridium-based single-photon superconducting detector as a fast detector for operation in the 0.1 K environment.

Due to the peculiar characteristics of iridium thin film, which has a Tc of 120-150 mK and resistivity to electron mean free path product that makes it suitable for low resistivity nanowires, we fabricated and studied SPSD samples in two types of geometries: small squares and high aspect ratio nanowires.

According to the detector models, measurements of electron-phonon coupling in metallic iridium are a key parameter to be studied to accelerate the detectors.

A systematic series of measurements with different sizes and geometries of electron-phonon conductivity is underway.

We present here the measurements, methodology and models, and preliminary results available.

Keywords: Transition Edge Sensor, Superconductivity, Single photon

ED3-5

Current-voltage characteristics of 100-pixel 200 μm square superconducting tunnel junction X-ray detector array

*Shigetomo Shiki[1], Go Fujii[1]

the National Institute of Advanced Industrial Science and Technology, Japan[1]

Superconducting tunnel junction (STJ) X-ray detector is promising for materials analysis because of its high energy resolution and high counting rate capability [1]. In order to achieve high sensitivity comparable to a silicon drift detector which has typical sensitive area of 10-100 mm^2, it is necessary to enlarge the size of an STJ pixel. We have fabricated 100-pixel STJ array with pixel size of 200 μm having layer structure of Nb-Al/AlOx/Al-Nb. Current – voltage (I-V) characteristics of 100-pixel STJ were measured more than 10 times at 0.3 K. Between each measurement, the temperature was raised more than Tc of Nb. Subgap current values at 0.3 mV were less than 10 nA in 90 pixels out of 100 pixels. The sensitivity of the 100-pixel STJ array is four times higher than in previous studies [1]. When comparing a series of IV curves focusing on a single pixel, the curves show several typical excesses. The fact suggests that the excess current is due to trapping of fluxoids. Possible sources of trapped magnetic fields are Ni plating of wiring materials and leakage of ambient magnetic fields through a magnetic shield. By reducing the residual magnetic field, larger sized STJs can be used.

[1] Shiki, S., Ukibe, M., Kitajima, Y. et al. X-ray Detection Performance of 100-pixel Superconducting Tunnel Junction Array Detector in the Soft X-ray Region. J Low Temp Phys 167, 748–753 (2012). https://doi.org/10.1007/s10909-012-0526-6

Keywords: Josephson junction, X-ray spectroscopy, Current-voltage characteristics

ED4-1-INV

Superconducting Nanowire Single-Photon Detectors

*Varun B Verma[1], Boris Korzh[2], Benedikt Hampel[1], Prasana Ravindran[1], Yao Zhai[1], Emma Wollman[2], Matthew Shaw[2], Richard Mirin[1], Sae Woo Nam[1]

NIST, USA[1]
JPL, USA[2]

Superconducting nanowire single-photon detectors (SNSPDs) are a class of superconducting single photon detectors combining high efficiency (>98% at 1550 nm), excellent timing resolution (~ 10s of ps), and ultra-low dark count rates (< 1 count/day). Historically, they have been widely used within the quantum optics community at telecommunications wavelengths in applications such as quantum computing and fundamental tests of quantum mechanics. Recently, we have developed SNSPDs operating at wavelengths extending into the mid-infrared from 2 – 10 microns. The mid-infrared is an important region of the spectrum for astronomy and chemical sensing, due to the unique spectral fingerprint of substances such as water vapor, carbon dioxide, carbon monoxide, ozone, and nitrous oxide. These molecules could be indicative of life on planets orbiting other stars, for instance. However, applications in astronomy will likely require large-format arrays of at least 1 kilopixel. While 1 kilopixel arrays were previously demonstrated by our group in the near-infrared, the multiplexing scheme cannot be used for mid-infrared-optimized SNSPDs. Recently, we have demonstrated a new multiplexing technique specifically for mid-infrared SNSPDs which relies on the thermal crosstalk between interleaved SNSPD pixels on suspended membranes. We will present the performance of 64 – pixel arrays as well as preliminary results on kilopixel-scale arrays. In addition, we will discuss the challenges involved in calibrating SNSPD detection efficiency in the mid-infrared spectrum, and will present a cryogenic system with integrated cryogenic spectrometer we have recently constructed for efficiency calibration. Finally, I will breifly discuss our recent development of SNSPDs integrated into ion traps for quantum computing applications.

Keywords: superconducting, detector, nanowire, photon

ED4-2-INV

Research and development of teraherz receivers in China

*Jian Chen[1,2], Lili Shi[1], Runfeng Su[1], Xuecou Tu[1,2,4], Jing Li[3], Jingbo Wu[1,2], Shengcai Shi[3], Peiheng Wu[1,2,4]

Nanjing University[1]
Purple Mountain Laboratories[2]
Purple Mountain Obvervatory[3]
Hefei Nantional Laboratory[4]

Recent progresses of terahertz (THz) receivers in China, are reported in this talk. The convenience THz reciever at room-temperature (RT) and high-sensetive superconducting THz recievers at low-temperature are desiged, fabricated and characterized. Nb_5N_6 microbolometer arrays with noise equivalent power (NEP) of 1.7×10^-11 W/Hz^0.5 and 64×64 pixels at 0.65 THz and RT have been constructed. Superconducting hot electron bolometer mixers with noise temperature of better than 8 times of quantum limitation have been obtained at several operating frequencies and 4.2 K. A superconducting hybrid NbTiN-Al kinetic inductance detector with NEP of about 2.6×10^-18 W/Hz^0.5 for phase readout at 4.3 THz and 200 mK has been characterized. Other THz detectors will been discussed also.

Keywords: Terahertz reciever, Microbolometer array, Hot electron bolometer mixer, Kinetic inductance detector

ED4-3

Low-energy single-electron detection using a large-area superconducting micro-strip

*Masato Shigefuji[1], Alto Osada[1,2], Masahiro Yabuno[3], Shigehito Miki[3,4], Hirotaka Terai[3], Atsushi Noguchi[1,5,6]

Komaba Institute for Science (KIS), The University of Tokyo, Japan[1]
PRESTO, Japan Science and Technology Agency, Japan[2]
Advanced ICT Research Institute, National Institute of Information and Communications Technology (NICT), Japan[3]
Graduate School of Engineering, Kobe University, Japan[4]
RIKEN Center for Quantum Computing (RQC), RIKEN, Japan[5]
Inamori Research Institute for Science (InaRIS), Japan[6]

Superconducting nano-strip single-photon detectors (SSPDs) [1] are excellent tools not only for photon detection but also for particle detection [2] owing to their high detection efficiency, low dark counts, and low time jitter. The detection mechanism relies on the heating of the electron subsystem in a superconductor by incident photons or particles. Interestingly, the former interact with electrons and excite quasiparticles directly, while the latter mainly excite phonons which heat electrons through the electron-phonon interaction. This difference results in a large difference in the minimum detectable energy: less than 1 eV for photons, on the other hand, ~ 600 eV for ions [3], both using a ~1 μm-wide stripline. From this point of view, the minimum detectable energy for electrons is interesting because electrons can interact with both electrons and phonons in a superconductor. However, the detection of low-energy electrons with a superconducting stripline has not been explored yet [4]. In this presentation, we show the detection property of superconducting micro-strip single-electron detectors (SSEDs) for electrons with energy under 152 eV.

As shown in Fig. (i), the SSED we use has a large detection area to increase the prospective angle from an electron source. We make use of the photoelectric effect as a low-energy electron source, and the photoelectrons are focused on the SSED using an einzel lens [Fig. (ii)]. The number of emitted electrons is estimated from the photocurrent, which is used to calculate the system detection efficiency (SDE).

We measure the dependence of the count rate of the SSED on the laser power and the result is shown in Fig. (iii). The count rate increases linearly with the laser power and depends on the applied voltages, indicating that photoelectrons are detected with our SSED. Then, as shown in Fig. (iv), we measure the SDE as a function of the kinetic energy of incident electrons. The result shows that in our experimental set-up, the minimum detectable energy for electrons is 15 eV, which is much lower than that of ions. This implies that electrons can transfer energy to the electron subsystem in a superconductor than ions by the electron-electron interaction. Our results show that SSEDs might open a wide range of applications ranging from condensed matter physics (e.g., quantum electron microscopy and cryogenic low-energy electron diffraction) to quantum information science (e.g., electrons in a Paul trap).

Captions for Figures
(i) (top) Optical micrograph of the SSED with a large active area of 420×420 μm^2 with a filling factor of 20 %. The NbTiN film is shown in pink. (bottom) Enlarged view. The superconducting

strip-line (orange) is 1 µm wide and 4 µm pitch.

(ii) Schematic cross-sectional view of the experimental set-up in a helium-3 refrigerator. The 390 nm-wavelength CW laser passes through the optical windows of the refrigerator and holes of two stainless steel meshes (not shown) and then is reflected by the mirror towards the calcium slab. Electrons are emitted by the photoelectric effect and accelerated towards the SSED. The initial potential energy of electrons is controlled by a voltage V_0. The electrons are focused on the SSED without changing the kinetic energy using an einzel lens with a voltage V_l (enclosed by the red dotted line).

(iii) Count rates for $V_0 = -100$ V, $V_l = 18$ V (red circles) and $V_0 = V_l = 0$ V (black squares) as a function of a 390 nm laser power P. A bias current of $I_b/I_{c,exp} \approx 0.98$ and a bias voltage of $V_d = 2$ V are applied to the SSED , where $I_{c,exp}$ is the experimental critical current. The error bars correspond to one standard deviation which originates principally in the fluctuation of the laser power.

(iv) SDE η_{sde} as a function of electron energy E_k for $V_l = 18$ V. The error bars represent one standard deviation. A bias current of $I_b/I_{c,exp} \approx 0.98$ and a bias voltage of $V_d = 2$ V are applied.

References

[1] G. Gol'tsman, O. Okunev, G. Chulkova, A. Lipatov, A. Semenov, K. Smirnov, B. Voronov, A. Dzardanov, C. Williams, and R. Sobolewski, "Picosecond superconducting single-photon optical detector," Applied physics letters 79, 705–707 (2001).

[2] R. Cristiano, M. Ejrnaes, A. Casaburi, N. Zen, and M. Ohkubo, "Superconducting nano-strip particle detectors," Superconductor Science and Technology 28, 124004 (2015).

[3] M. Sclafani, M. Marksteiner, F. M. Keir, A. Divochiy, A. Korneev, A. Semenov, G. Gol'tsman, and M. Arndt, "Sensitivity of a superconducting nanowire detector for single ions at low energy," Nanotechnology 23, 065501 (2012).

[4] M. Rosticher, F. Ladan, J. Maneval, S. Dorenbos, T. Zijlstra, T. Klapwijk, V. Zwiller, A. Lupaşcu, and G. Nogues, "A high efficiency superconducting nanowire single electron detector," Applied Physics Letters 97, 183106 (2010).

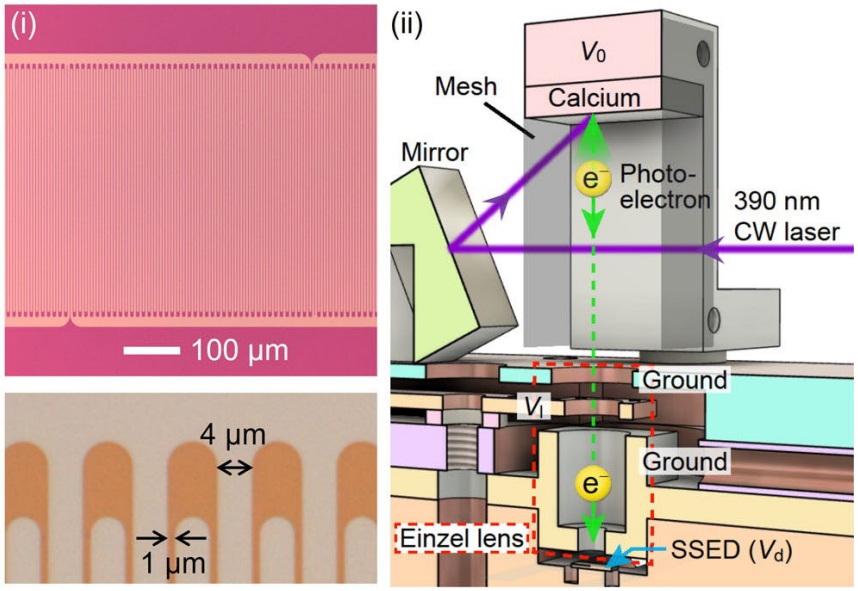
(i)
100 µm
4 µm
1 µm
(ii)
V_0
Calcium
Mesh
Mirror
e⁻
Photo-electron
390 nm CW laser
Ground
V_1
Ground
e⁻
Einzel lens
SSED (V_d)

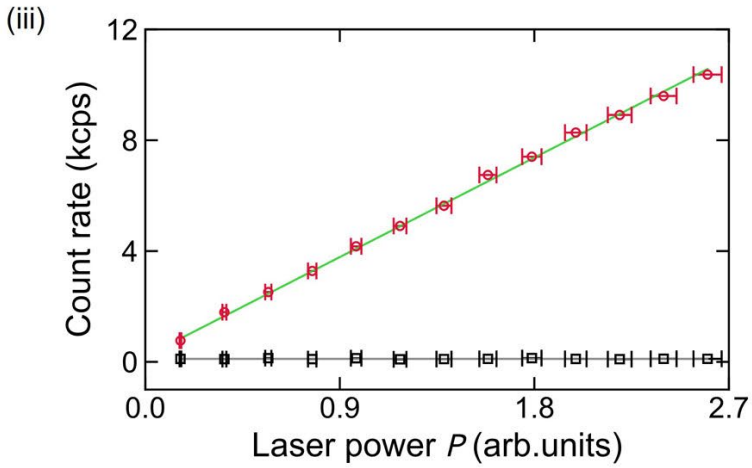
(iii)
Count rate (kcps)
12
8
4
0
0.0
0.9
1.8
2.7
Laser power P (arb.units)

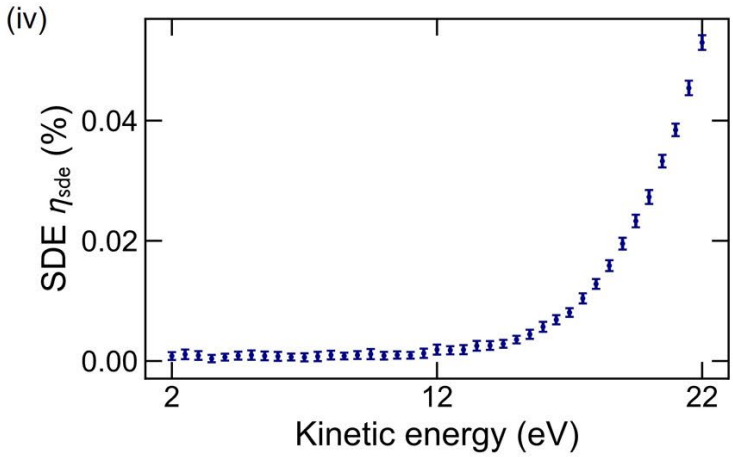
(iv)
SDE η_{sde} (%)
0.04
0.02
0.00
2
12
22
Kinetic energy (eV)

ED4-4

Superconducting neutron transmission imaging for investigating a sequential change in phase separations of low-melting Wood's metal

*The Dang Vu[1,2], Hiroaki Shishido[3], Kazuya Aizawa[2], Takayuki Oku[2], Kenichi Oikawa[2], Masahide Harada[2], Kenji M. Kojima[4], Shigeyuki Miyajima[5], Kazuhiko Soyama[2], Tomio Koyama[1], Mutsuo Hidaka[6], Soh Y. Suzuki[7], Manobu M. Tanaka[8], Masahiko Machida[9], Shuichi Kawamata[1], Takekazu Ishida[1]

Division of Quantum and Radiation Engineering, Osaka Metropolitan University, Sakai, Osaka 599-8570, Japan[1]
Materials and Life Science Division, J-PARC Center, Japan Atomic Energy Agency, Tokai, Ibaraki 319-1195, Japan[2]
Department of Physics and Electronics, Graduate School of Engineering, Osaka Metropolitan University, Sakai, Osaka 599-8531, Japan[3]
Centre for Molecular and Materials Science, TRIUMF, 4004 Wesbrook Mall, Vancouver, BC V6T 2A3, Canada[4]
Advanced ICT Research Institute, National Institute of Information and Communications Technology, 588-2 Iwaoka, Nishi-ku, Kobe, Hyogo 651-2492, Japan[5]
Advanced Industrial Science and Technology, Tsukuba, Ibaraki 305-8568, Japan[6]
Computing Research Center, Applied Research Laboratory, High Energy Accelerator Research Organization (KEK), Tsukuba, Ibaraki 305-0801, Japan[7]
Institute of Particle and Nuclear Studies, High Energy Accelerator Research Organization (KEK), Tsukuba, Ibaraki 305-0801, Japan[8]
Center for Computational Science & e-Systems, Japan Atomic Energy Agency, 178-4-4 Wakashiba, Kashiwa, Chiba 277-0871, Japan.[9]

Superconducting detectors have superior advantages in achieving high sensitivity, fast response, and high energy resolution. In the past decades, they have been successfully applied to a superconducting nanowire single photon detector (SNSPD), a transition edge sensor (TES), and a microwave kinetic conductance detector (MKID). We first proposed the idea of a superconducting sensor called a current-biased kinetic inductance detector (CB-KID) [1].The CB-KID has a significant difference from others because it utilizes a voltage signal coming from a sudden change in a kinetic inductance of a hot spot in a superconducting meanderline under feeding a modest DC bias current and its low-loss propagation along a superconducting stripline. We need a netron conversion ^{10}B layer to detect charge-neutral neutrons. A delay-line technique makes it possible to conduct the neutron transmission imaging in two dimensions only with the four-terminal CB-KID device. The detector has been systematically investigated to understand its characteristics and to optimize the operating conditions for improving the spatial resolution, the temporal resolution, and the detection efficiency [2,3]. The practical usefullness tests were done with various samples in view of good linearity between the Gd-islands sizes evaluated not only by neutron images but also by SEM images over the wide range of sample sizes [4], a demonstration of the narrow-area Bragg-edge neutron transmission [5], the Bragg-dip analyses for observing mosaic structure in a SmSn mixed metal [6], and the confirmation of spatial resolution down to 16 mm [7].

In this study, we used a delay-line-CB-KID measurement system to obtain a microstructure of Wood's metal alloy (Bi 50%, Pb 25%, Sb 12.5%, Cd 12.5%, melting temperature 75.2°C) under beam power of 812 kW at beamline BL10 of J-PARC (MLF). The Wood's metal is composed of four

phases, of which one is a Cd-rich needle-like phase of an average width of 25 μm and length of 5 mm. Since Cd is a strong neutron absorber, it is suitable for observing the fine mosaic structure contrastingly by neutron transmission imaging. We modified our cryostat system to be able to mount a room-temperature sample for conducting the experiments under pulsed neutrons. After neutron-transmission imaging with the Wood's metal at its initial state, we melted the Wood's metal sample and sodified it again by slow cooling during the same beam time. We were successful in observing an impressive change in morphorogy of the phases by neturon-transmission imaging.

Since CB-KID is a cryogenic detector, the sample to be investigated has been located near the CB-KID sensor at an operating temeperature. Neutron imaging by CB-KID with cryogenic-temperature samples is not so convenient for users to exchange a sample and to conduct the open beam normalization of imaging in a limited beam time. Room-temperature sample imaging achieved in the present study would be very useful to apply our CB-KID system to versatile different samples of interest in the future.

This work is partially supported by Grant-in-Aid for Scientific Research (A) (No. JP21H04666) and Grant-in-Aid for Early-Career Scientists (No. JP21K14566) from JSPS. The neutron irradiation experiments at the Materials and Life Science Experimental Facility (MLF) of the J- PARC were conducted under the support of MLF project program (No. 2021P0501).

References

[1] Ishida T, *et al.,* 2014 Toward mega-pixel neutron imager using current-biased kinetic inductance detectors of Nb nanowires with 10B converter *J. Low Temp. Phys.* 176 216–221

[2] Vu T D, *et a*l. 2019 Temperature dependent characteristics of neutron signals from a current-biased Nb nanowire detector with 10B converter *J. Phys.: Conf. Ser.* 1293 012051

[3] Vu T D, *et al*. 2020 Kinetic inductance neutron detector operated at near critical temperature *J. Phys.: Conf. Ser.* 1590 012036

[4] Vu T D, *et al*. 2021 Practical tests of neutron transmission imaging with a superconducting kinetic-inductance sensor *Nucl. Instrum. Meth. Phys. Res. A* 1006 165411

[5] Vu T D, *et al*. 2022 Narrow-area Bragg-edge transmission of iron samples using superconducting neutron sensor *J. Phys.: Conf. Ser*. 2323 012028

[6] Shishido H, *et al.* 2022 Neutron Imaging toward Epithermal Regime using a Delay Line Current-Biased Kinetic-Inductance Detector *J. Phys.: Conf. Ser.* 2323 012029

[7] Iizawa Y, *et al.* 2019 Energy-resolved neutronvimaging with high-spatial resolution using a superconducting delay-line kinetic inductance detector *Supercond. Sci. Technol.* 32 125009

Keywords: Superconducting neutron detector, CB-KID, Neutron, Wood's metal

ED4-5

Crystalline Orientation of CaF_2 window determined by Neutron Transmission Imaging using a Delay Line Current-Biased Kinetic-Inductance Detector

*Hiroaki Shishido[1,2], The Dang Vu[3,4], Kazuya Aizawa[4,8], Kenji M. Kojima[3,5], Tomio Koyama[3], Kenichi Oikawa[4], Masahide Harada[4], Takayuki Oku[4], Kazuhiko Soyama[4], Shigeyuki Miyajima[6], Mutsuo Hidaka[7], Soh Y. Suzuki[8], Manobu M. Tanaka[9], Shuichi Kawamata[3], Takekazu Ishida[3]

Department of Physics and Electronics, Graduate School of Engineering, Osaka Metropolitan University[1]
The Center for Research and Innovation in Electronic Functional Materials, Osaka Metropolitan University[2]
Division of Quantum and Radiation Engineering, Osaka Metropolitan University[3]
Materials and Life Science Division, J-PARC Center, Japan Atomic Energy Agency[4]
Centre for Molecular and Materials Science, TRIUMF and Stewart Blusson Quantum Matter Institute, University of British Columbia[5]
Advanced ICT Research Institute, National Institute of Information and Communications Technology[6]
Advanced Industrial Science and Technology[7]
Computing Research Center, Applied Research Laboratory, High Energy Accelerator Research Organization (KEK)[8]
Institute of Particle and Nuclear Studies, High Energy Accelerator Research Organization (KEK)[9]

Several useful properties of superconducting devices are applicable to fulfilling high-sensitivity superconducting detectors [1]. We developed a superconducting detector, named as a current-biased kinetic-inductance-detector (CB-KID), which particularly *targets applications in neutron beams* [2].

CB-KID consists of two orthogonal *X* and *Y* superconducting Nb meanderlines and a Nb ground plane. This superconducting stripline structure guarantees long-distance electromagnetic wave propagation of a signal. In addition, a ^{10}B neutron conversion layer is deposited on top of the CB-KID to utilize a ^{7}Li particle and a ^{4}He particle emitted toward opposite directions accompanying with the nuclear reaction between incident neutrons and ^{10}B atoms. When one of them excites temporary quasiparticles locally at a hotspot on the *X* and *Y* meanderlines, a transient change of the kinetic inductance under a small DC-bias current produces a pair of voltage pulses which is in proportional to a time derivative of the kinetic inductance and DC-bias current, and propagates toward both ends of the meanderlines as electromagnetic waves. We record signal arrival timestamps with a temporal resolution of 1 ns by using a high-speed time-to-digital converter (TDC) of the Kalliope-DC circuit. Since a signal-arrival-time difference at both ends can be used to identify the hotspot position, thus a neutron transmission image is determined in two-dimensions with high spatial resolution from signal arrival timestamps of a signal quartet in two meanderlines by a delay-line method. We call the combination of CB-KID and delay-line method as a delay-line CB-KID system.

A pulsed neutron source is characterized to generate a wide energy range of neutrons simultaneously at a regular repetition intervals (25 Hz at J-PARC). Generated neutrons fly through a beamline of a certain length *L* and are separated by energy according to the time of flight. Thanks to high temporal resolution and multi-hit tolerance of delay-line CB-KID, energy-resolved neutron-transmission measurements and imaging are conveniently achievable. For single crystal samples, of which the neutron scattering cross section has a sufficiently large fraction in the total

cross section, the wavelength dependence of the neutron transmission spectrum tends to show dip structures associated with Bragg diffractions. The wavelength of the Bragg dip is determined by the crystalline orientation of the single crystal and the index of reflection.

CaF_2 has a CaF_2-type face-centered cubic structure and is often used as an optical window. CaF_2 window has various properties depending on how they are cut. The CaF_2 window (15 mm 2 mm^{t}) used for the present study was cut in a random-crystalline orientation. We measured neutron transmission images and transmission spectra for a CaF_2 single crystal using pulsed neutrons with a source size D = 100 mm at BL10 NOBORU of the Material and Life science experimental Facility (MLF), J-PARC [3]. The sample was placed at 20 mm upstream side from the detector at room temperature in air. The detector was kept at 5 K during the neutron irradiation experiments under beam power of 711 kW and the collimator ratio of L/D = 140.

We observed dip structures in the neutron transmission spectrum of the CaF_2 single crystal sample. The Miller indices were successfully assigned for the observed Bragg dips, and thus we were able to determine the crystal orientation of the CaF_2-window sample. We also identified dip structures due to nuclear resonance absorption of Ca and F nucleus in the energy range of epithermal neutrons. The combination of delay-line CB-KID with ^{10}B converter and pulsed neutron source is applicable to Bragg-dip analysis and identification of constituent nuclei by the nuclear resonance absorption in a non-destructive manner.

This work is partially supported by Grant-in-Aid for Scientific Research (A) (No. JP21H04666) and Grant-in-Aid for Early-Career Scientists (No. JP21K14566) from JSPS. The neutron irradiation experiments at the Materials and Life Science Experimental Facility (MLF) of the J- PARC were conducted under the support of MLF project program (No. 2021P0501).

[1] K. D. Irwin, *Appl. Phys. Lett.* 66, 1998 (1995); P. K. Day *et al*., *Nature* 425, 817 (2004); J. Zmuidzinas, *Annu. Rev. Condens. Matter Phys.* 4, 169 (2012).
[2] T. Ishida *et al*., J. Low Temp. Phys. 176, 216 (2014); H. Shishido *et al*., Appl. Phys. Lett. 107, 242601 (2015); H. Shishido *et al*., Phys. Rev. Appl. 10, 0440440 (2018); Y. Iizawa *et al*., Supercond. Sci. Technol. 42, 125009 (2019).
[3] K. Oikawa *et al*., Nucl. Instrum. Methods Phys. Res. A 589, 310 (2008).

Keywords: Superconducting detector, Neutron transmission spectroscopy, CB-KID

ED5-1-INV

High Performance HTS Multi-Band Microwave Bandpass Filters Using Multimode Resonators

*Baoping Ren[1], Xuehui Guan[1], Haiwen Liu[2], Zhewang Ma[3]

East China Jiaotong University[1]
Xi'an Jiaotong University[2]
Saitama University[3]

High-temperature superconducting (HTS) microwave bandpass filters (BPFs) have advantages of extreme low insertion loss, high selectivity of passbands, and high rejected-level in stopband. On the other hand, multimode resonators can provide multiple resonances and exhibit the same behaviors with several single-mode resonators, which highly reduce the circuit size. In past few years, we engaged in the development of high performance and compact HTS multi-band microwave BPFs by using multimode resonators, such as the square ring loaded resonator and hairpin ring resonator. Furthermore, differential/balanced filters are widely used in modern communication systems for their good common-mode (CM) rejection capability, which results in higher immunity to the environmental noise and electromagnetic interference as compared with their single-ended counterparts. So, a series of HTS multiband differential/balanced microwave BPFs with deep suppression of common-mode noise signal were developed by adopting multimode resonators. With the advantages of ultra-low in-band insertion losses and high CM suppression, the demonstrated filters are attractive for potential applications in multiband communication systems requiring high-sensitivity and high anti-interference properties.

Keywords: bandpass filter, differential circuits, multimode resonators, multi-band

ED5-2-INV

Propagation in Superconducting Niobium Rectangular Waveguide in the 100 GHz band

*Tac Nakajima[1], Kazuji Suzuki[1], Takafumi Kojima[2], Yoshinori Uzawa[2], Masayuki Ishino[3], Issei Watanabe[4]

Institute for Space-Earth Environmental Research, Nagoya University, Japan[1]
National Astronomical Observatory of Japan, Japan[2]
Kawashima Manufacturing Co., Ltd., Japan[3]
National Institute of Information and Communications Technology, Japan[4]

Receivers of a radio telescope for astronomy and atmospheric radiometer for earth science in the millimeter/sub-millimeter bands are usually used complicated waveguide circuits such as a sideband-separating unit (e.g. Claude et al. 2000), an ortho-mode transducer (e.g. Moorey et al. 2006), and a multiplexer (e.g. Kojima et al. 2017). However, if these waveguide components are placed before the superconducting tunnel junction device (SIS mixer) or HEMT amplifier, which is the first detector in the receiver system, the system noise increases due to the transmission loss of the waveguide circuit. This effect is a serious problem, especially in the sub-millimeter and the terahertz-wave band. Even in the international radio astronomical observatory project namely the Atacama Large Millimeter/sub-millimeter Array (ALMA) multiband receiver covering 35 to 950 GHz, the dual polarization and sideband-separating receiver based on waveguide technique is a limited frequency range of up to 500 GHz. Above this frequency, waveguide components placed in front of the detector are being developed with an emphasis on how to avoid transmission loss.

Rectangular waveguides that use superconducting materials for the waveguide walls, that is, superconducting waveguides, are expected to reduce transmission loss compared to normal metal waveguides. However, research on the superconducting waveguides has been limited so far, especially on the fabrication and measurement of physical models in the mm/sub-mm band. For this reason, the effectiveness of superconducting waveguides in reducing transmission loss and system noise has not been clarified. Therefore, we have attempted to fabricate superconducting niobium (Nb) rectangular waveguide in the 100 GHz band, measure its propagation characteristics, and verify its effectiveness.

In this work, the resonator method is adopted for the measurement of waveguide propagation because accurate measurement of a short waveguide at cryogenic temperature is quite difficult. First, we fabricated the Nb rectangular waveguide resonator in the 100 GHz band. However, Nb is known as a difficult-to-machine material, and many metal-processing companies lack experience in its fabrication. Thus, we started to search for the best cutting tools and machining conditions. As a result, we succeeded in fabricating the waveguide with a surface accuracy of 0.3 μm (RMS) using an end mill with a diameter of 1 mm. For comparison, the same waveguide resonators made of aluminum alloy (A6061; hereafter Al) and tellurium copper (with a gold finish; hereafter Au) were fabricated as representative waveguide materials (upper side of the figure).
Next, we measured those resonance characteristics at room temperature, 298 K, and cryogenic temperature, 4.8 K (lower side of the figure). The resonance properties of all materials at 298 K are almost consistent with the shapes predicted from the literature-based conductivities. On the other hand, at 4.8 K, the changes in the resonance properties of superconducting Nb are significantly larger compared to that of Al and Au. We used electromagnetic analysis software to

reproduce these properties and calculated electrical conductivity and propagation loss. The conductivity of Al, Au, and Nb at 4.8 K are calculated as 5.2×10^{7} S/m, 2.8×10^{8} S/m, and 1.1×10^{11} S/m, respectively. The propagation loss of the Nb waveguide per meter is estimated as 0.06 dB/m, and this value is approximately 1/30 that of Al and 1/17 that of Au.
In this presentation, we will report details of the discussion on propagation loss and the effectiveness of superconducting rectangular waveguides.

Keywords: Superconducting Waveguide, Niobium, millimeter-wave, Radio Astronomy

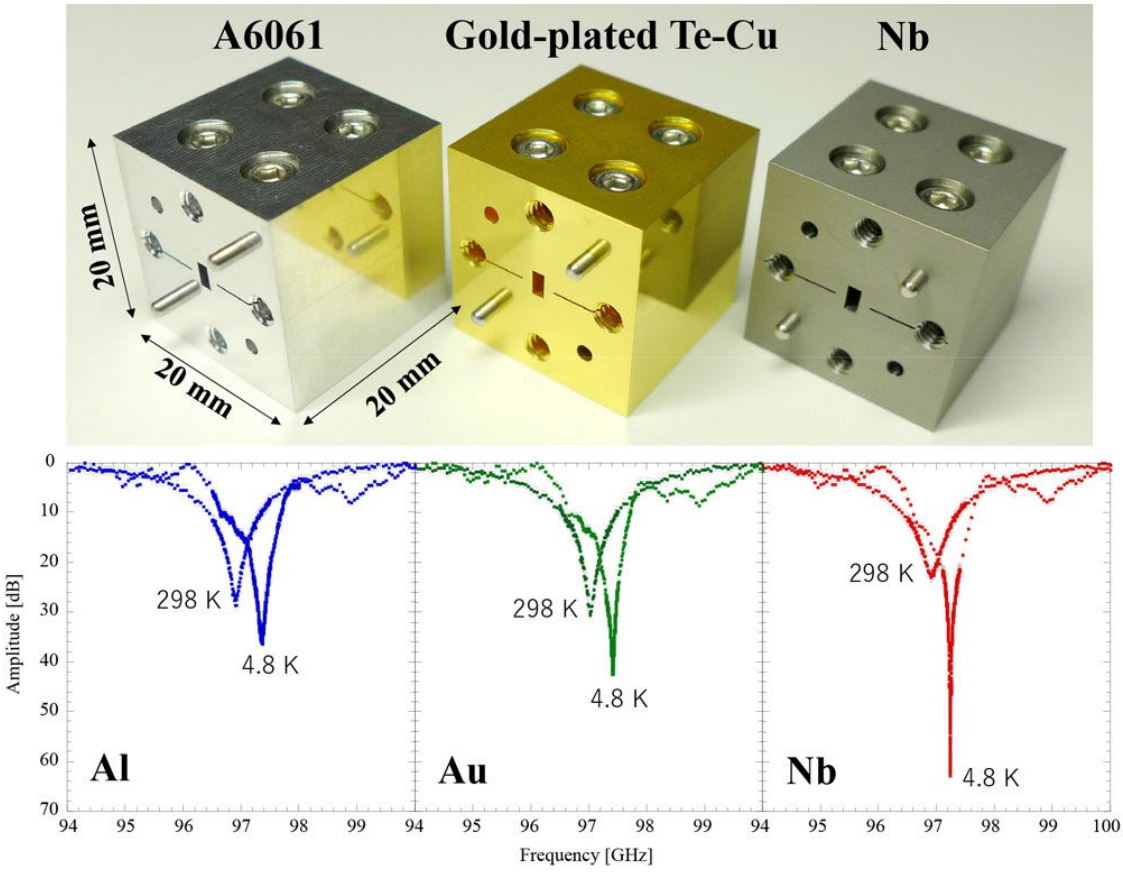

ED5-3

Magnetic interference and current distribution of cross-type and overlap-type Josephson junctions exposed to oblique magnetic fields

*Tenma Ueda[1], Edmund Soji Otabe[1], Yasunori Mawatari[2]

Kyushu Institute of Technology (Japan)[1]
National Institute of Advanced Industrial Science and Technology (Japan)[2]

The gauge-invariant phase difference in a Josephson junction is modulated by the magnetic field and the magnetic field dependence of the DC critical current shows a Fraunhofer-like interference pattern. Magnetic interference is an important phenomenon in applications of superconducting quantum interference devices. It has been reported that the overlap-type junctions show magnetic interference of critical currents under perpendicular magnetic fields [1], whereas cross-type junctions do not [2]. In addition, it has been numerical investigated that interference patterns are strongly dependent on the arrangement of the superconducting strips [3].

In this study, we analytically show the magnetic interference of critical currents and Josephson current density through the barrier layer in cross-type and overlap-type junctions under applying oblique magnetic fields. We assume that the self-field and the magnetic screening is sufficiently small. Figure 1 shows the parallel Φ_x and perpendicular magnetic field Φ_z dependence of critical currents I_c normalized by maximum critical current I_{c0} in overlap-type junction. Figure 2 shows the Josephson current density distribution J_z (x,y) in the barrier layer normalized by the critical current density J_c in overlap-type junction. By comparing these results for cross-type and overlap-type junctions, we consider how the strips arrangements and the junction geomety affect the magnetic interference of critical currents.

[1] I. Rosenstein and J. T. Chen, Phys. Rev. Lett. 35, 303 (1975).
[2] S. L. Miller, K. R. Biagi, J. R. Clem, and D. K. Finnemore, Phys. Rev. B 31, 2684 (1985).
[3] R. Monaco, M. Aaroe, J. Mygind, and V. P. Koshelets, J. Appl. Phys. 104, 023906 (2008).

Fig.1: Logarithmic density plot of the critical current $I_c(\Phi_x,\Phi_z)/I_{c0}$ as a function of the parallel Φ_x/Φ_0 and perpendicular magnetic flux $\Phi z/\Phi_0$ in overlap-type junctions.

Fig. 2: Logarithmic density plot of Josephson current density $J_z(x,y)/J_c$ in overlap-type junctions for Φ_x/Φ_0=0 and Φ_z/Φ_0=4.

Keywords: Josephson effect, magnetic interference, overlap-type junction, cross-type junction

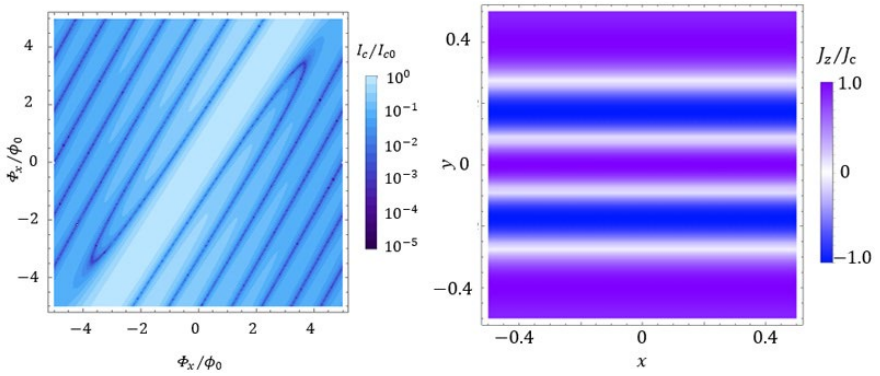

ED5-4

Simulation study of magnetic shielding effects for operation on a Josephson voltage standard device in a high magnetic field

*Daiki Matsumaru[1], Shuji Nakamura[1], Michitaka Maruyama[1], Nobu-Hisa Kaneko[1]

The National Institute of Advanced Industrial Science and Technology (Japan)[1]

The Josephson effect has been utilized for primary voltage standards, since it can generate precise voltage guaranteed by quantum mechanics [1]. In the primary Josephson voltage standard (JVS) systems, dedicated dewars filled with liquid helium or mechanical cryocoolers with magnetic shielding and low-noise wiring are considered indispensable, which prevents us to directly use the quantized voltage signals for the other low temperature measurements without signal cables passing through the room temperature environments.

High quality voltage references in cryogenic conditions will be utilized for precise electrical measurements in basic physics and metrology fields [2]. In the series of our study, we have been trying to realize stable reference voltage sources in low temperatures and high magnetic fields conditions by implementing an optimally-shielded JVS device in a dilution refrigerator.

In our previous study, we developed a temperature-control module for the JVS device implemented on the 4 K stage of a dilution refrigerator, and confirmed generation of quantized voltages with stable temperature control under no magnetic field condition [3]. In this presentation, we report the optimized design and simulation of the effects of magnetic shields on the JVS device operation under a magnetic field. Our target is to reduce the residual magnetic field inside the shields to the level lower than the magnitude of the geomagnetic field, i.e., approximately 50 μT, even with an external high magnetic field. In the simulation, we assumed 10 T magnetic field generated by a superconducting magnet mounted at the bottom of the mixing chamber stage of the refrigerator. Given the calculation, we reached the optimal combination of shielding materials (high-magnetic-permeability metal/Pb/Nb) and thicknesses of them, the box of which showed that the simulated residual magnetic field in the vicinity of the JVS can reduce to less than 10 μT. A prototype magnetic shield box based on the simulation result has been fabricated, and it will be experimentally confirmed the performance.

This work was supported by JSPS KAKENHI Grant Number JP18H05258.

[1] M. Maruyama, A. Iwasa, H. Yamamori, S.-F. Chen, C. Urano, and N.-H. Kaneko, “Calibration System for Zener Voltage Standards Using a 10 V Programmable Josephson Voltage Standard at NMIJ, ” IEEE Trans. Instrum. Meas., vol. 64, no. 6, pp. 1606−1612, Jun. 2015.

[2] T. J. B. M. Janssen, J. M. Williams, N. E. Fletcher, R. Goebel, A. Tzalenchuk, R. Yakimova, S. Lara-Avila, S. Kubatkin, and V.I. Fal'ko, “Precision comparison of the quantum Hall effect in graphene and gallium arsenide, ” Metrologia, vol. 49, no. 3, pp. 294−306, Mar. 2012.

[3] D. Matsumaru, S. Nakamura, Z. Jia, M. Maruyama, and N.-H. Kaneko, “Operation of a Josephson voltage standard device cooled with a dilution refrigerator,” ISS2021 Conf. Digest, pp. 1−1, Nov. 2021.

Keywords: Josephson effect, voltage standard, magnetic shielding, magnetic field

ED5-5

Ginzburg-Landau simulation of the three-terminal operations of a superconducting-nanowire cryotron

*Naoki Yasukawa[1], Taichiro Nishio[1], Yasunori Mawatari[2]

Tokyo University of Science (Japan)[1]
National Institute of Advanced Industrial Science and Technology (Japan)[2]

Superconducting single flux quantum (SFQ) digital circuits can operate at high speed with lower power consumption, whereas complementary metal oxide semiconductor (CMOS) circuits are very compatible with conventional technology. By combining SFQ and CMOS circuits, it is expected to realize super high-performance hybrid devices. However, output from SFQ circuits is too small to drive semiconductor circuits, and therefore, additional devices as interfaces to communicate each other are required.

A superconducting nano-wire cryotron (nTron) which was invented by MIT is a three-terminal device, and its basic operating principle is the current-driven transition from the superconducting state to the normal state. Its applications are expected as the interfaces of superconductor-semiconductor hybrid devices, superconducting detectors, and quantum-computing devices. Although the nTron's fundamental characteristics are getting clear, we still need to understand its physical mechanism and operation characteristics.

We have developed the numerical technique to simulate the three-terminal operation of the nTron by using the finite element method to solve the time-dependent Ginzburg-Landau (TDGL) equation and thermal diffusion equation. Specifically, we first apply the finite gate current and sweep the channel bias current, and we investigate (channel-bias current)-(channel-voltage) characteristics of the nTron.

The direct-current operation model was successfully reproduced experimental data by MIT, and we made sure that direct-current injection from the gate can control channel voltage to induce the normal state transition. Further, we investigated the pulse-wave response of the nTron to understand the behavior of channel state when a pulse current was injected from the gate.

This work was supported by JSPS KAKENHI Grant Numbers JP20K05314.
We thank N. Yoshikawa for the helpful discussions about the nTron's operation.

Keywords: superconducting nanowire cryotron, Ginzburg-Landau simulation, hybrid devices

ED6-1-INV

3D packaging technology for superconducting circuits

Kazumasa Makise[1,2]

National Astronomical Observatory of Japan[1]
National Institute of Advanced Industrial Science and Technology[2]

Three-dimensional packaging of superconducting quantum bits and superconducting circuits is one of the most important technologies for large scale superconducting circuits. Therefore, we proposed multi-chip 3D packaging technology to realize scalable superconducting devices. Such a multi-chip technology is used to implement to complex large circuits. In this report, we will discuss superconducting 3D packaging technology focusing on two points: flip chip and Through Silicon Via (TSV).

First, a superconducting connection using a flip chip is described. Superconducting solder bumping test chips were designed for daisy-chain connection circuit. The test devices consist of a top chip and a base chip. Nb/Ti/Au contact pads for placing were fabricated on Si substrates. To obtain electrical properties of a large number of interconnects, we design and fabricate over 10000 circular lead solder bumps from 10 to 50 um diameter on the top chip and Nb/Ti/Au-opposing-contact pads on the base chip to form a daisy chain of about 10000 chip-to-chip interconnects. We chose lead as the solder material because it has a relatively high critical temperature of 7.2 K and we can check superconducting connection using liquid He and/or conventional refrigerators.

Next, superconducting TSVs are explained. There is a method for accessing a two-dimensional array of qubits with microwaves from the vertical direction, which requires the use of TSVs to realize a waveguide-like structure. In this case, instead of embedding TSVs, the sides are homogeneously covered with a superconducting thin film. There are several ways to do this, such as long-throw sputtering and tilting the substrate, but we have used atomic layer deposition (ALD). Specifically, we evaluated the transport properties of TiN films deposited by thermal and plasma ALD, and optimized the deposition conditions. The principle is that raw material gas is injected from the upper shower head onto the TSV substrate, and the metal decomposed by the heat and plasma is transferred to the substrate and the gas is exhausted to the exhaust side. Homogeneity and crystallinity of the ALD-TiN film on the TSV substrate were evaluated. Cross-sectional SEM and STEM images of the TSV substrate showed that TiN films with a thickness of approximately 100 nm were homogeneously deposited in the vertically formed vias to the back side of the substrate. The electron diffraction image of TiN on the TSV wall shows a clear diffraction ring, and the measured lattice spacing is consistent with that of TiN. These diffraction rings were observed at various parts of the TSV, suggesting that a homogeneous TiN film with crystallinity was deposited inside the TSV. The superconducting transition temperature of this film was measured to be 3 K. It was also found that the composition of Ti and N differs between the upper side of the TSV, which is exposed to the plasma, and the lower side, which is not. The correlation between the composition distribution and superconducting properties should be investigated to make the composition uniform.

ED6-2-INV

3D integration of superconducting chips with through silicon vias

*Martin Weides[1], Nicholas Nugent[1], Jharna Paul[1], Valentino Seferai[1], James Grant[1], Tania Hemakumara[3], Yi Shu[3], Dmytro Besprozvannyy[3], Russ Renzas[3], Myunglae Jo[2], Tobias Lindstrom[2]

The University of Glasgow[1]
National Physical Laboratory[2]
Oxford Instruments[3]

The next generation of superconducting quantum devices requires both 3D integration and reduced loss. While early devices in the field have been mainly made with Nb and Al, these materials have lossy surface oxides. They are incompatible with conformal deposition techniques required for superconducting through silicon vias. Superconducting nitrides have emerged as a compelling alternative due to their potential for reduced surface oxide-induced loss and compatibility with conformal deposition techniques such as Atomic Layer Deposition (ALD). While TiN has been thoroughly studied with sputtering and CVD, little work has been published with ALD or promising alternative nitrides such as NbN, NbTiN, and TaN.

In this work, we have developed a process for the fabrication of superconducting resonators and superconducting through silicon vias using NbN deposited with plasma-enhanced ALD. We report Tc, measured internal quality factors, and our novel ALD-based approach to superconducting TSV fabrication. Our results clearly demonstrate that ALD superconducting nitrides are promising and practical alternatives for next-generation 3D integrated low-loss superconducting quantum devices.
*We acknowledge funding from Innovate UK ISCF Quantum Technologies, NPL and EPSRC iCASE.

Keywords: Qubit, vertical integration, Through silicon via

ED6-3

Factorization circuit composed of 32-superconducting flux qubits utilizing the quantum annealing

*Daisuke Saida[1,2], Mutsuo Hidaka[1], Fuminori Hirayama[1], Yuki Yamanashi[3]

The National Institute of Advanced Industrial Science and Technology (Japan)[1]
Fujitsu Limited (Japan)[2]
Yokohama National University (Japan)[3]

The quantum computer has a potential to reduce computation time compared to classical ones for certain problems. Typical example of the problem is the prime factorization. Shor's algorithm is widely recognized to solve the prime factorization effectively [1]. However, to implement this algorithm in the gate-type quantum computer requires the large numbers of qubits with sufficient fidelity. Another candidate method uses quantum annealing (QA), where the prime factorization is treated as an optimization problem with solutions as the global minimum of the Hamiltonian [2]. In this method, classical computation is required to calculate the Gröbner basis, which helps to reduce the cost function. We have investigated an alternative method that can solve the prime factorization by QA directly. In our method, the superconducting quantum circuit with a function of the Multiplier unit (MU) is utilized [3,4]. The circuit of MU performs factorization of two digits in binary. Using the connection qubit (CQ), carry transfer is possible between MUs [5]. With a combination of the MUs and CQs, it is expected that a highly scalable quantum circuit can be created. In this work, we demonstrate the 4-bit factorization circuit composed of 4-MUs. The quantum annealing circuit is fabricated by using a process that creates four Nb layers and a Josephson junction with a critical current density of 1 μA/μm^2. In the device design and analysis of its performance, a Josephson integrated circuit simulation (JSIM) was utilized [6]. Experiment was carried out both at 4.2-K and 10-mK. The qubits used in this experiment are superconducting compound Josephson junction rf-SQUID flux qubits[3,4].

The MU_{ij} (i = 0-1, j = 0-1) is composed of 6-superconducting flux qubits with all-to-all connectivity. Six qubits (X_{ij}, Y_{ij}, Z_{ij}, D_{ij}, C_{ij}, S_{ij}) correspond to the X_{ij} and Y_{ij} for inputs, Z_{ij} for sum-in, D_{ij} for carry-in, C_{ij} for carry-out, and S_{ij} for summation. To accomplish the carry transfer between MUs, 8-CQs are utilized. An inductance of each CQ was designed so that it would not fail in carry transfer. Our 4-bit factorization circuit is consisted by 32-superconducting flux qubits. Input (X, Y) and output (P) relationship is expressed by $X = X_{01}X_{00}$, $Y = Y_{11}Y_{01}$ and $P = C_{11}S_{11}S_{10}S_{00}$ (binary notation). The JSIM analysis was carried out with 100 iterations in order to estimate a success probability of the factorization. Solutions of $(10)_2 \times (10)_2$ and $(11)_2 \times (11)_2$ were successfully obtained in cases of the annealing with $P = (0100)_2$ and $P = (1001)_2$, respectively. In the annealing with $P = (0110)_2$, solutions of $(10)_2 \times (11)_2$ and $(11)_2 \times (10)_2$ were clearly obtained. Similar combinations of X and Y were also confirmed in the experiment.

Acknowledgements
This work is partly funded by the NEC-AIST Quantum Technology Cooperative Research Laboratory. This work is partly based on results obtained from a project commissioned by the New Energy and Industrial Technology Development Organization (NEDO), Japan (project number JPNP16007). The devices were fabricated in the clean room for analog-digital superconductivity (CRAVITY) in National Institute of Advanced Industrial Science and Technology (AIST).

References

[1] Shor, W. Polynomial-time algorithms for prime factorization and discrete logarithms on a quantum computer. *SIAM J. Comput*. 26, 1484-1509 (1997).

[2] Dridi, R. & Alghassi, H. Prime factorization using quantum annealing and computational algebraic geometry. *Sci. Rep*. 7, 43048 (2017).

[3] Saida, D. et al. Experimental demonstrations of native implementation of Boolean logic Hamiltonian in a superconducting quantum annealer. *IEEE Trans. Quant. Eng*. 2, 3103508-3103515 (2021).

[4] Saida, D. et al. Factorization by quantum annealing using superconducting flux qubits implementing a multiplier Hamiltonian. *Sci. Rep*. 12, 13669 (2022).

[5] Saida D. et al, Quantum annealing with native implementation of Hamiltonian in the multiplier unit, *ISS2021*, ED7-6.

[6] Fang, E. S., & Van Duzer, T., A Josephson Integrated Circuit Simulator (JSIM) for superconductive electronics application. in *Proc. Ext. Abstr. 2nd Int. Supercond. Electron. Conf*., 407 (1989).

Keywords: quantum computer, quantum annealing, superconducting flux qubit, prime factorization

ED6-4

Nitride-based superconducting coplanar waveguide resonator with an internal quality factor above one million

*Paniz Foshat[1], Paul Baity[1], Sergey Danilin[1], Valentino Safari[1], Shima Poorgholam-khanjari[1], Mingqi Zhang[1], Oleg A. Mukhanov[2], Matthew Hutchings[2], Robert Hadfield[1], Muhammad Imran[1], Martin Weides[1], Kaveh Delfanazari[1]

University of Glasgow (United Kingdom)[1]
SeeQc (United Kingdom)[2]

As a type II superconductor, niobium nitride (NbN) has been widely used in quantum circuits [1-2]. Insensitivity to magnetic fields and high kinetic inductance make it a suitable material candidate for applications in complex superconducting quantum circuits. However, NbN is more susceptible to decoherence sources such as two-level system (TLS) defects, and optimising the fabrication procedure is one of the main challenges which should be overcome. Here, we investigate microwave photonic losses in NbN-based superconducting quantum circuits. Our circuits consist of an array of microwave resonators made from a 100 nm thin NbN film, capacitively coupled to a common coplanar waveguide. We designed, modelled, and optimised the resonators on various substrates such as Sapphire and intrinsic Silicon (Si) through analytical calculations and numerical simulations. We microfabricated the NbN resonators on Si and performed the microwave measurements at cryogenic temperatures down to T = 80 mK. We study the internal quality factor (Qi) of fabricated microwave resonators in millikelvin temperature in the power range of -140 dBm to -95 dBm. We further show an agreement between numerical calculation and measured internal quality factor at T = 100 mK.

We report results for one of our samples, which includes three resonators, each with 4 µm widths and 2 µm gap, coupled to a feed line, all formed on a 525 µm thick Si substrate. The Si substrate was cleaned with HF solution to remove any native oxide before sputtering NbN. The resonators are fabricated using standard e-beam lithography and CF4 anisotropic dry etch. The resonator length was chosen to have a fundamental frequency mode between 3-6 GHz (see Fig.1 a, for results for one resonator). We observed that at low temperature (T = 100 mK), the internal quality factor increases from Qi = 1.4×10^5 ±4.7×104 in the single photon regime to Qi = $10^6\pm1.4\times10^5$ at high powers (Fig.1.b). We further found an agreement between the estimated TLS losses and our experimental results [2].

[1] Carter, Faustin W., et al *Applied Physics Letters* 115.9 (2019): 092602.
[2] Probst, Sebastian, et al. *Review of Scientific Instruments* 86.2 (2015): 024706.

Keywords: Superconducting resonator, Two level system (TLS) loss

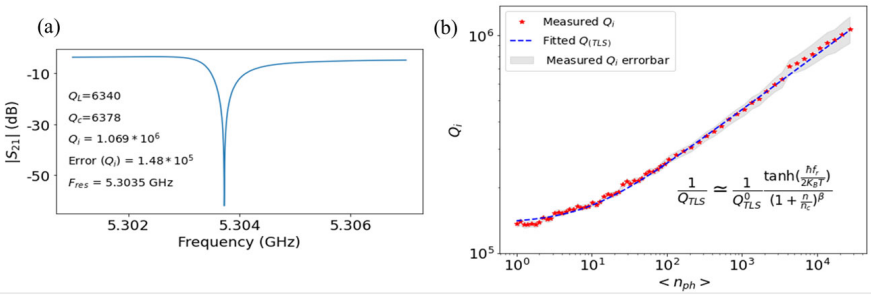

FIG.1 (a) Frequency spectrum of one of the resonators with Q_c = 6378, loaded quality factor Q_L = 6340, and internal quality factor Q_i = 10^6 at T = 100 mK and P = -95 dbm. (b) Internal Quality factor as a function of average photon

ED6-5

Quantum Key Distribution on Microwave band for superconducting quantum computing

*Mingqi Zhang[1], Paniz Foshat[1], Shima Poorgholam[1], Muhammad Imran[1], Martin Weides[1], Kaveh Delfanazari[1]

James Watt School of Engineering, University of Glasgow, United Kingdom[1]

We propose a quantum key distribution (QKD) system operating at cryogenic temperature to build secure microwave wireless link between quantum computers. One of the state-of-the-art methods of building high quality quantum computers is based on superconducting technology. Limited by the microwave components working at cryogenic temperature, the frequencies of superconducting quantum computing are generally from f=4GHz to f=10GHz. So building quantum secure link at this frequency range at cryogenic temperature is important for the accomplishment of private quantum communication.

Continuous Variable (CV) QKD is one way to build secure link depending on quantum mechanics. We consider a one-way light-of-sight (LOS) point to point microwave communication link between two users: Alice and Bob. The process of this scheme is as follow: Alice starts from a single thermal state and prepares coherent states from a two-dimensional Gaussian distribution. Then she sends her states to Bob through an insecure diffraction-only channel with transmissivity T. Bob uses a homodyne detection to measure the income states and get the outcome. To examine the security of this link, we assume the attacker Eve hiding in the channel and operating collective attack to steal information. To minimize risk of leakage, Alice and Bob carry out privacy amplification in the post-processing and use reverse reconciliation (RR) to prepare their secret key.

In conclusion, this work focuses on the secure wireless distance between different superconducting quantum computers' communication systems by using microwave CVQKD. The results may benefit the communication systems between both quantum computers and inter-satellite.

Reference:
[1] Zhang, M., Foshat, P., Poorgholam Khanjari, S., Imran, M. , Weides, M. and Delfanazari, K. Microwave Quantum Key Distribution with Cryogenic Microwave Components for Superconducting Quantum Computing. 2022 International Symposium on Quantum Computing: Circuits Systems Automation and Applications (QC-CSAA), Knoxville, TN, USA, 18-19 July 2022

Keywords: Quantum Key Distribution (QKD), Microwave, Quantum Communication, Cryogenic Components

ED7-1-INV

Fabrication Process Development for Very Large-Scale Superconductor Integrated Circuits: Progress, Challenges, and Limitations

*Sergey K Tolpygo[1]

Lincoln Laboratory, Massachusetts Institute of Technology[1]

Superconductor electronics provides tremendous advantages in information processing speed and energy dissipation in comparison to semiconductor electronics, offering clock rates in excess of 100 GHz, energy dissipation below 10^{-19} J per bit, and essentially dissipationless data transfer. The main factor impeding wide-spread implementation of superconductor electronics, both classical and quantum, is a relatively low scale of integration. Presently, the device count and the device number density in SICs reach, respectively, about 10^6 active devices (Josephson junction) per circuit and about 10^7 devices per cm^2. This integration scale is about 3 to 4 orders of magnitude lower than in the most advanced, 3-nm and 5-nm, CMOS technology nodes, resulting in a much lower functionality of superconductor integrated circuits (SICs) compared to CMOS circuits.

In order to clarify the physical and technological factors limiting the scale of integration, I will briefly review the main types of superconducting logics: a) Single Flux Quantum (SFQ) logics encoding information by magnetic flux quanta and utilizing ultrafast switching of Josephson junctions, and b) parametric logics (nSQUID, AQFP) utilizing quasi-adiabatic changes in the flux state of logic cells. Despite some differences, all superconducting logics share the same scaling relations, whereas each of them has its unique poorly scalable components.

I will review the most advanced fabrication processes developed for superconductor electronics at MIT Lincoln Laboratory and the process development being done in order to increase integration scale of superconductor electronics by a factor of 10x to 100x in the near future. In particular, replacement of essentially geometrical Nb inductors in logic cells by compact NbN or/and NbTiN kinetic inductors; transition from the current fabrication node using 248-nm deep-UV photolithogrpahy with 250 nm minimum linewidth to the 150-nm node using 193-nm photolithography; replacement of presently used externally shunted Nb/Al-AlO_x/Nb Josephson junctions with critical current densities, J_c, of 100 μA/μm^2 and 200 μA/μm^2 by self-shunted junctions with J_c = 600 μA/μm^2; and increasing the number of superconducting layers from nine to ten. I will also briefly discuss and present recent results of our efforts to develop damascene processing of superconductor ICs, using plasma enhanced chemical vapor deposition of superconducting films over narrow trenches and contact holes (vias) with subsequent planarization by metal chemical mechanical polishing.

Keywords: superconductor integrated circuit, Josephson junction, AQFP, SFQ

ED7-2-INV

Extremely energy-efficient integrated circuit technology beyond the thermodynamic limit

*Nobuyuki Yoshikawa[1], Taiki Yamae[1], Naoki Takeuchi[1,2]

Yokohama National University[1]
National Institute of Advanced Industrial Science and Technology (AIST)[2]

Reversible logic circuit, which conserves the thermodynamic entropy during calculation, is an extremely energy-efficient logic circuit. Their energy consumption approaches zero in the quasistatic operation limit if the erasure of the information does not happen. Therefore, the energy consumption can be reduced even lower than the thermal limit $k_B T \ln 2$, known as the Landauer limit [1]. We proposed that the reversible logic gate can be realized based on the adiabatic quantum flux parametron (AQFP) and named it the reversible quantum flux parametron (RQFP) [2][3]. In this presentation, we will show our latest progress in this study. After introducing the operation principle of the RQFP gate, we will discuss the origin of energy consumption in reversible and irreversible logic circuits. We have designed and demonstrated several RQFP logic circuits, including an 8-bit ripple carry adder, 4-to-16 decoder, and flip-flops. Simulation results of the RQFP circuits indicate that their energy consumption is lower than those based on irreversible AQFP logic when the operation frequency is reduced and even lower than the Landauer limit. The perspective of the reversible circuits based on AQFP will be shown.

[1] N. Takeuchi, Y. Yamanashi, N. Yoshikawa, “Reversible logic gate using adiabatic superconducting devices,” Scientific Reports, 4, 6354 (2014).
[2] N. Takeuchi, Y. Yamanashi, N. Yoshikawa, “Reversibility and energy dissipation in adiabatic superconductor logic,” Scientific Reports, 7, 75-1-12 (2017).
[3] R. Landauer, “Irreversibility and Heat Generation in the Computing Process,” IBM J. Res. Develop. 5, 183–191 (1961).
[4] T. Yamae, N. Takeuchi, N. Yoshikawa, “A reversible full adder using adiabatic superconductor logic,” Supercond. Sci. Technol. 32, 035005 (2019).

Keywords: Digital

ED7-3-INV

Next-Generation Cryogenic/Superconducting Computer Architectures

*Jangwoo Kim[1]

Seoul National University[1]

On facing the end of multi-core performance and DVFS scaling, computer architects now suffer from critical challenges to further improve the performance and power efficiency with conventional room-temperature computing. To overcome the challenge, architects are now aiming to exploit cryogenic/superconducting computing in which they operate computer devices at extremely low temperatures to maximize their operation frequency with their static power consumption minimized. However, to realize the new computers by developing low-temperature optimized computers and applying them to the real field, architects are in dire need of the low-temperature device modeling and architecture simulation methodologies and should show the successful architecture and system examples.

In this work, I will first introduce the potential of cryogenic/superconducting computing from the perspective of a computer architect. Next, I will explain our modeling methodology which can accurately measure the performance and power consumption of cryogenic/superconducting computer devices and architectures. Finally, I will cover various architecture examples designed to take advantage of the target low temperatures. Among the varoius cryogenic/superconduncting architecture examples, I will focus on our recent work to develop a fault-tolerant large-scale quantum control processor built with low-temperature devices.

Keywords: Cyrogenic computing, Superconducting computing, Computer architecture, Architecture modeling

ED7-4

Evaluation of True Random Number Sequences Generated by Utilizing Timing Jitters in Superconducting Integrated Circuits

*Kenta Sato[1], Naonori Sega[1], Hiroshi Shimada[1], Yoshinao Mizugaki[1]

The University of Electro-Communications, Japan[1]

SFQ circuitry is attractive to next-generation integrated circuits because it realizes high-speed operation and low power consumption. A Hardware Random Number Generator (HRNG) is one of the applications in SFQ circuitry. Random number sequences are used in various fields such as simulations of natural phenomena and cryptographical communication. Especially, an HRNG, which generates true random number sequences having complete randomness, is required in fields related to information security. True random number sequences are generated by using physical phenomena such as noise, collapse, and chaotic dynamics. In SFQ circuitry, thermal noises in Josephson junctions and shunt resistors induce non-negligible jitters for circuits' operation. Onomi et al. studied SFQ HRNGs that generated true random number sequences utilizing timing jitters by thermal noise, and they operated an HRNG in which the trigger signal had timing jitters longer than the period of a high-frequency Josephson oscillator.

In this research, we proposed an HRNG with two oscillators to enhance stability against variation of oscillator frequencies. We investigated the characteristics of random numbers generated by the proposed HRNG not only by numerical simulation but also by experiments using test circuits fabricated a Nb/AlOx/Nb integration process.

Figure 1 shows a simplified block diagram of the HRNG we designed. We use two oscillators, a Clock Oscillator, and a Gate Oscillator. The oscillators are oscillated by the over-biasing method: a DC voltage is applied to the Josephson junction. The signal from the Clock Oscillator is transferred to the reset terminal of a Non-Destructive Read-Out memory (NDRO), and the clock and input terminals of an XOR gate. Then the signal from the Gate Oscillator is fed to another input terminal of the XOR gate. Signals of two oscillators are fed to the XOR gate with timing jitters, and therefore, the output of the XOR gate becomes truly random. The generated random number is stored in the NDRO, and the random number is obtained from the Output by feeding a Trigger signal at arbitrary time.

The numerical simulation soft we used was JoSIM. Figure 2 shows the Gate Oscillator frequency f_{gate} dependence of the probability of "1" for four Clock Oscillator frequencies f_{clk} at Trigger frequency f_{trig} of 6.31 GHz. The black dashed lines indicate edges for passing Monobit test in the random number test FIPS 140-2. It shows that the probability of "1" is the local minimum at $f_{clk} \cong f_{gate}$. Figure 3 shows the f_{clk} and f_{gate} dependence of three categories of the pass rate of the FIPS 140-2 at f_{trig} = 6.31 GHz. The oscillators' frequency conditions for 100% pass rate agree with the conditions for the probability of "1" being in 48.625%-51.375%. Figure 4 shows the f_{trig} dependence of the pass rate of FIPS 140-2 at f_{clk} = 40 GHz and f_{gate} = 69.2 GHz. It operated up to f_{trig} = 10 GHz.

We designed the HRNG using the Nb 10kA/cm^2 process. Figure 5 shows the voltage wave-form converted from SFQ signals generated by the HRNG. Table 1 shows the result of the random number test SP800-22, which is a stricter test than FIPS140-2, for 50 samples of 20 kbits random number sequences generated at f_{trig} = 1 MHz, f_{clk} = 48.79 GHz, and f_{gate} = 19.81 GHz. It shows the results of 9 in 15 tests were "Success". On the other hand, "Rank", "RandomExcursions", "RandomExcursionsVariant", and "LinearComplexity" tests were "Fail" because the length of random number sequences was too short, while "Universal" test was known to be unsuitable.

Keywords: Superconducting integrated circuit, SFQ circuit, Hardware random number generator, True random number

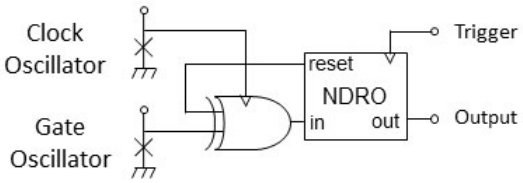

Fig. 1

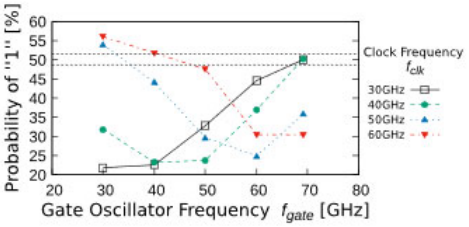

Fig. 2

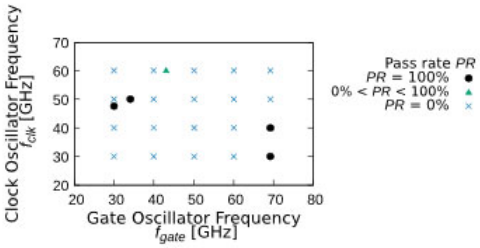

Fig. 3

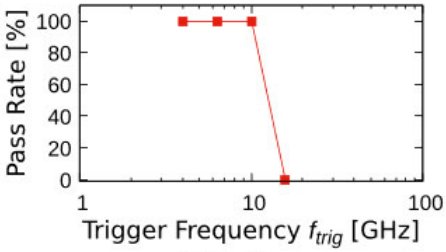

Fig. 4

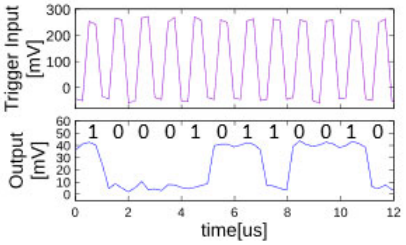

Fig. 5

Tab. 1

Test name	P-value	Fail Rate	
Frequency	0.616305	0	Success
BlockFrequency	0.075719	2	Success
CumulativeSums	0.534146	0	Success
Runs	0.419021	2	Success
LongestRun	0.213309	2	Success
Rank	0.040108	4	Fail
FFT	0.289667	0	Success
NonOverlappingTemplate	0.147342	1.47	Success
OverlappingTemplate	0.001757	0	Success
Universal	0	100	Fail
ApproximateEntropy	0.000199	16	Fail
RandomExcursions	N/A	N/A	Fail
RandomExcursionsVariant	N/A	N/A	Fail
Serial	0.534146	2	Success
LinearComplexity	0.935716	4	Fail

ED7-5

Possibility of using the pinning phenomenon of superconductors as a reservoir computing

*Ken Arita[1], Tenma Ueda[1], Edmund S Otabe[1], Yuki Usami[1], Hirofumi Tanaka[1], Tetsuya Matsuno[2]

Kyusyu Institute of Technology (Japan)[1]
National Institute of Technology, Ariake College (Japan)[2]

Reservoir computing, which takes advantage of physical phenomena with nonlinearities, is attracting a lot of attention. In fact, such physical reservoir computing has attracted increasing attention in diverse fields of research [1]. Therefore, we turned our attention to superconductivity, a physical phenomenon with nonlinearities between the electric field and the current density. Compared to other physical phenomena used in reservoirs, we believe that superconductivity can easily adjust the nonlinearity by pin placement to produce dynamics suitable for reservoirs.
First, the time-dependent Ginzburg-Landau equation was solved numerically with Affine Integrator (AFI) [2] to visualize the motion of magnetic flux lines. The results are shown in Fig. 1. Then, the nonlinearity between the electric field generated by the motion of the magnetic flux lines and the input current density was used to perform a reservoir computing task. Three tasks were performed: a waveform generation task, a Nonlinear Autoregressive Moving Average (NARMA)2 task, and a nonlinear-memory task, and it was observed that the waveforms of the predictions followed the target waveforms. These results clearly show that superconductivity has enough important characteristics to be used as a reservoir. The results of the NARMA2 task are shown in Fig. 2. The first possible cause for the success of the tasks is the flux pinning interaction. The relationship between the *E-J* property of superconductivity and the pinning of magnetic flux is a well-known part of the superconductivity. This sudden generation of an electric field creates a nonlinearity. Another possible cause is the reversible motion of the magnetic flux lines. This one is mainly related to memorability. It is thought that memorability results from the inclusion of stored energy in the energy density during reversible motion inside the pin.

[1]Yuki Usami, Bram van de Ven, Dilu G Mathew, et al. Advanced Materials, 33(48):2102688, 2021.
[2] T. Matsuno, E.S. Otabe, Y. Mawatari, J.Phys. Soc. Japan 89 (2020) 054006.

Fig. 1: Motion of magnetic flux lines. The magnitude and phase of the order parameter are represented by luminance and hue.
Fig. 2: Result of the NARMA2 task. Red is the target, blue is the prediction during learning, and green is the prediction after learning.

Keywords: Reservoir computing, Nonlinearity, Pinning

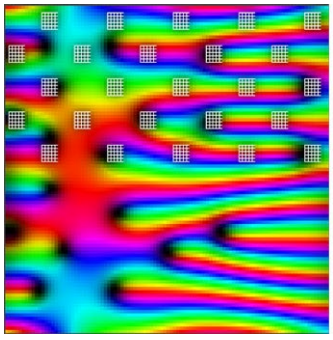

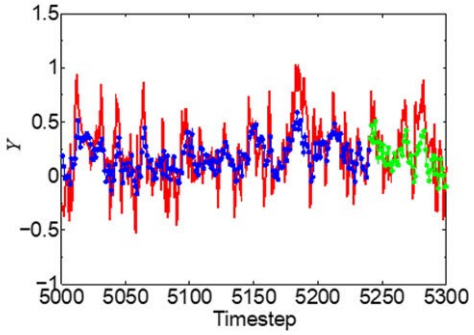

ED7-6

Accuracy Improvement of Polynomial Computing RSFQ Circuits Based on Stochastic Computing by Partial Duplication

Moeka Tsuji[1], Nobutaka Kito[1]

Chukyo University (Japan)[1]

Rapid-Single-Flux-Quantum (RSFQ) circuits are gaining attention as ultra-fast and low-power computing devices. This circuit represents logic values with voltage pulses. Each logic gate in RSFQ circuits is a clocked gate. In other words, each gate has a clock input terminal and outputs a calculation result as a presence or absence of a pulse for every clock period.

Recently, stochastic computing (SC) is attracting attention in both CMOS circuit designs and superconducting circuit designs. SC is suitable for applications tolerating small error such as neural network processing. A value in SC is represented by a ratio of 1's in a bit-stream on a wire. Namely, in RSFQ circuits, a value in SC is represented by the number of pulses on a wire during observed clock periods. SC can realize multiplication with an AND gate. It is possible to realize a small area arithmetic circuit with SC. Though the number of clock cycles to observe increases as the calculation precision increases, duplicating an SC circuit, in other words, preparing copies of the original circuit and observing their output bit-streams, can reduce the number of clock cycles.

This presentation proposes a design method of stochastic computing circuits with improved accuracy by partial duplication. The method extends the design method of calculation circuits of polynomials in [1] to improve accuracy by duplication. Polynomials can represent many useful arithmetic functions. Though duplication can improve accuracy, naïve duplication increases circuit area largely. This method reduces the area overhead of duplication by sharing an internal part among the original and copies.

The method in [1] designs a circuit for calculating a polynomial from a transformed polynomial. The method transforms a polynomial considering available operations in SC such as multiplication with an AND gate and subtraction-from-one with a NOT gate and generates a transformed formula for designing a circuit. The transformed formula can be calculated by a circuit in which AND gates and NOT gates are connected alternately. An AND gate locates at the output of a circuit designed with the transformed formula. The proposed method duplicates only the AND gate at the output of the circuit. Duplicated units in the designed circuit share most of the original circuit.

Several circuits computing polynomials have been designed with the proposed method and evaluated by simulation. The mean absolute error of a circuit calculating the Maclaurin series of sine functions was reduced to 78% from a circuit designed with the original method in [1] with the same number of clock cycles.

Reference

[1] Koki Wada and Nobutaka Kito 2022 *J. Phys.: Conf. Ser.* 2323 012032.

Keywords: stochastic computing, RSFQ circuit